

HEART DISEASE

Cold shock domain–containing protein E1 is a posttranscriptional regulator of the LDL receptor

Geoffrey A. Smith^{1†‡}, Arun Padmanabhan^{2,3,4†}, Bryan H. Lau⁵, Akhil Pampana^{6,7}, Li Li⁸, Clara Y. Lee^{2,3,4}, Angelo Pelonero⁴, Tomohiro Nishino⁴, Nandhini Sadagopan^{2,3,4}, Vivian Q. Xia^{3,9}, Rajan Jain^{8,10}, Pradeep Natarajan^{6,7,11}, Roland S. Wu^{2,3,5§}, Brian L. Black⁵, Deepak Srivastava^{4,12,13}, Kevan M. Shokat^{1,14}, John S. Chorba^{3,9*}

Copyright © 2022 The Authors, some rights reserved; exclusive licensee American Association for the Advancement of Science. No claim to original U.S. Government Works

The low-density lipoprotein receptor (LDLR) controls cellular delivery of cholesterol and clears LDL from the bloodstream, protecting against atherosclerotic heart disease, the leading cause of death in the United States. We therefore sought to identify regulators of the LDLR beyond the targets of current therapies and known causes of familial hypercholesterolemia. We found that cold shock domain–containing protein E1 (CSDE1) enhanced hepatic *LDLR* messenger RNA (mRNA) decay via its 3' untranslated region and regulated atherogenic lipoproteins *in vivo*. Using parallel phenotypic genome-wide CRISPR interference screens in a tissue culture model, we identified 40 specific regulators of the LDLR that were not previously identified by observational human genetic studies. Among these, we demonstrated that, in HepG2 cells, CSDE1 regulated the LDLR at least as strongly as statins and proprotein convertase subtilisin/kexin type 9 (PCSK9) inhibitors. In addition, we showed that hepatic gene silencing of *Csde1* treated diet-induced dyslipidemia in mice to a similar degree as *Pcsk9* silencing. These results suggest the therapeutic potential of targeting CSDE1 to manipulate the posttranscriptional regulation of the *LDLR* mRNA for the prevention of cardiovascular disease. Our approach of modeling a clinically relevant phenotype in a forward genetic screen, followed by mechanistic pharmacologic dissection and *in vivo* validation, may serve as a generalizable template for the identification of therapeutic targets in other human disease states.

INTRODUCTION

The low-density lipoprotein receptor (LDLR) delivers cholesterol from LDL to cells to maintain membrane homeostasis (1). By clearing atherogenic LDL particles from the bloodstream, the hepatic LDLR protects against atherosclerotic heart disease (2). Despite successful therapies that up-regulate the hepatic LDLR and reduce heart attacks, such as 3-hydroxy-3-methylglutaryl coenzyme A reductase (HMGCR) inhibitors (statins), Neimann-Pick C1-like (NPC1L1) inhibitors, or proprotein convertase subtilisin/kexin type 9 (PCSK9) inhibitors (3), cardiovascular disease remains the leading cause of death in Western countries (4). Lowering LDL beyond that achieved by statins improves clinical outcomes without adverse effects (5). Although there is a theoretical concentration at which LDL concentrations could get

too low (6), this has yet to be found in large randomized trials (7). Whether other LDLR regulatory mechanisms could be leveraged to further treat heart disease remains unknown.

The genetics of familial hypercholesterolemia (FH), which manifests as an isolated elevation in serum LDL, underlies the clinical success of LDLR up-regulation by statins and PCSK9 inhibitors. Estimates suggest that 20 to 40% of FH phenotypes remain unexplained outside of the four major causes: *LDLR*, apolipoprotein B (*APOB*), *PCSK9*, and LDLR adaptor protein 1 (*LDLRAP1*) (8). Although polygenic causes drive some unexplained phenotypes (9–11), additional regulators of the LDLR may still exist. Advances in forward genetics using clustered regularly interspaced short palindromic repeats (CRISPR)–based technologies (12–14) can now enable searches for tissue- and disease-specific effects across the entire genome that may elude the sporadic natural variants found in observational studies, which themselves require compatibility throughout the entire life span and in all cell types. Moreover, hepatic delivery of gene silencing agents has been shown to be effective in the clinic (15), providing a therapeutic modality against hits whose phenotypes are driven by expression in the liver. We therefore used a genome-wide CRISPR interference (CRISPRi) screen for factors involved in hepatic LDLR regulation, both to understand the biology of this important receptor and to uncover potential therapeutic targets in cardiovascular disease.

RESULTS

A genome-wide CRISPRi screen for LDLR regulation

We engineered the HepG2 cell line, which models the regulation of the LDLR (16–20), to constitutively express an inactive Cas9 protein fused to the Krüppel-associated box transcriptional repressor (dCas9-KRAB), enabling the knockdown of any given gene with an appropriate single guide RNA (sgRNA; Fig. 1A) (12, 13). Because

¹Department of Cellular and Molecular Pharmacology, University of California, San Francisco, San Francisco, CA 94158, USA. ²Division of Cardiology, UCSF Health, San Francisco, CA 94143, USA. ³Department of Medicine, University of California, San Francisco, San Francisco, CA 94143, USA. ⁴Gladstone Institute of Cardiovascular Disease, San Francisco, CA 94158, USA. ⁵Cardiovascular Research Institute, University of California, San Francisco, San Francisco, CA 94158, USA. ⁶Cardiovascular Research Center, Massachusetts General Hospital, Boston, MA 02114, USA. ⁷Program in Medical and Population Genetics, Broad Institute of Harvard and MIT, Cambridge, MA 02142, USA. ⁸Department of Medicine and Penn Cardiovascular Institute, University of Pennsylvania, Philadelphia, PA 19104, USA. ⁹Division of Cardiology, Zuckerberg San Francisco General Hospital, San Francisco, CA 94110, USA. ¹⁰Department of Cell and Developmental Biology, Institute of Regenerative Medicine, and Penn Epigenetics Institute, University of Pennsylvania, Philadelphia, PA 19104, USA. ¹¹Department of Medicine, Harvard Medical School, Boston, MA 02114, USA. ¹²Departments of Pediatrics and Biochemistry and Biophysics, University of California, San Francisco, San Francisco, CA 94143, USA. ¹³Roddenberry Center for Stem Cell Biology and Medicine at Gladstone, San Francisco, CA 94158, USA. ¹⁴Howard Hughes Medical Institute, University of California, San Francisco, San Francisco, CA 94143, USA. *Corresponding author. Email: john.chorba@ucsf.edu

†These authors contributed equally to this work.

‡Present address: Dana-Farber Cancer Institute, Boston, MA 02215, USA.

§Present address: Amgen, South San Francisco, CA 94080, USA.

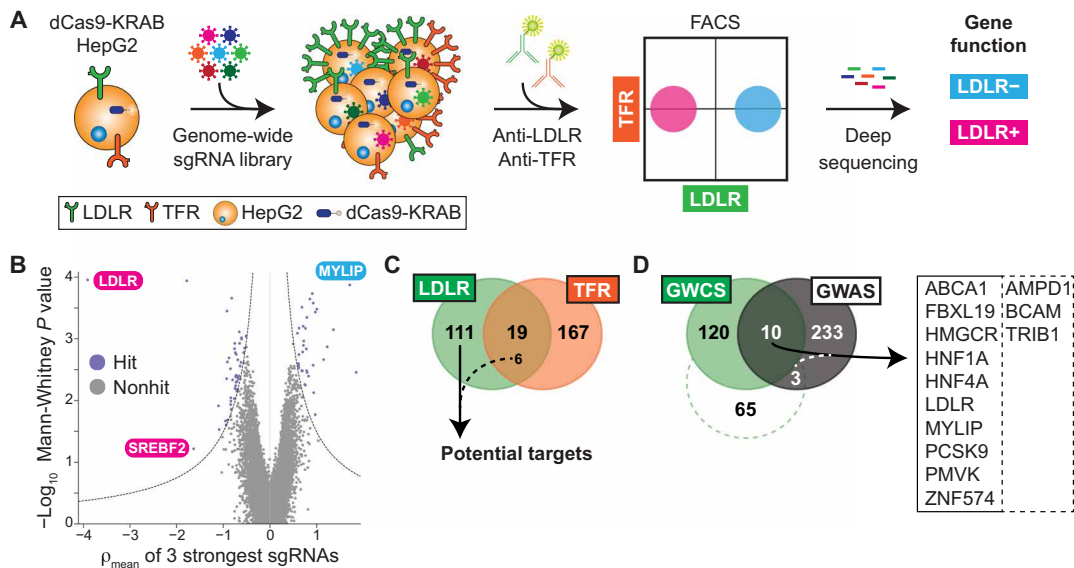


Fig. 1. Results from the genome-wide CRISPRi screen. (A) Overall schematic of phenotypic selection. CRISPRi-ready cells are transduced with a genome-wide library of sgRNAs, surface-labeled with antibody, sorted by flow cytometry, and deep sequenced to deconvolute putative gene functions. See main text for details. (B) Volcano plot showing the statistical significance (Mann-Whitney test) of the guides recovered for each gene against the mean ρ phenotype of the three guides with the strongest effect. ρ is defined as the \log_2 fold enrichment for sgRNAs recovered from cells with high-LDLR abundance cells to those recovered from cells with low LDLR abundance. Guides targeting known regulators of the LDLR are noted. (C) Venn diagram showing the overlap between parallel LDLR and TFR screens. Six guides common to both had opposing abundance phenotypes in the respective screens and were included as specific hits. (D) Venn diagram of hits between the LDLR genome-wide CRISPRi screen (GWCS) and putative genes correlated with serum LDL cholesterol (LDL-C) from GWAS. The dotted line indicates a relaxed threshold for hit selection from LDLR screen, with only an additional three genes in the overlap. Overlap genes shown at the right.

statins (21) and PCSK9 inhibitors (22–24) increase cell surface LDLR, we scored surface LDLR abundance. To focus on factors that preferentially affect LDLR abundance over other receptors, we performed a parallel screen for regulators of the transferrin receptor (TFR). This critical player in iron metabolism shares a clathrin-mediated intake mechanism but is otherwise orthogonally regulated from the LDLR (25, 26). Before our screen, we confirmed dCas9-KRAB activity (fig. S1A) and an appropriate dynamic range for both LDLR and TFR regulation by transduction with sgRNAs expected to alter receptor abundance in either direction. For LDLR, we targeted *LDLR* and myosin regulatory light chain interacting protein (*MYLIP*), which encodes an E3 ligase that ubiquitinates the LDLR and causes lysosomal degradation (fig. S1B) (27). For TFR, we targeted *TFRC* and zinc finger CCCH-type containing 12A (*ZC3H12A*), which encodes an endoribonuclease that degrades *TFRC* mRNA (fig. S1C) (28).

We next performed our pooled screens in parallel by transducing a library encoding sgRNAs with fivefold coverage of the entire protein-coding human genome (13). We selected the cells at the upper and lower third of receptor abundance by fluorescence-activated cell sorting (FACS) and quantified the sgRNAs for each population via deep sequencing (fig. S2, A to F, and tables S1 to S4). We compared the degree of enrichment of LDLR or TFR surface amounts in the high-abundance to the low-abundance cells (defined as ρ ; Fig. 1B). We also compared the cells with high and low receptor abundance to the unsorted population (defined as τ or γ , respectively) and included these results in our final hit count. This resulted in 130 total hits for the LDLR and 186 hits for the TFR (tables S5 and S6). We hypothesized that hits with shared phenotypes would likely have global effects on surface receptors, leaving us with 117 hits specific

for LDLR regulation (Fig. 1C and table S5). Gene ontology (GO) analysis (29) revealed a 15-fold enrichment for cholesterol metabolism as a biologic process (11 total hits; $P = 5.7 \times 10^{-10}$), providing confidence that we recapitulated our target biology. The hits also included 48 members of potentially druggable protein classes, including 29 with proposed enzymatic activity, and 22 hits were unclassified in GO databases (fig. S3A).

Cross-referencing human genetic datasets identifies LDLR regulators in vivo

We next compared genes associated with serum LDL cholesterol (LDL-C) from published genome-wide association studies (GWAS) (30–32) to our list of hits. However, only 13 of these genes overlapped with our results (Fig. 1D), even when we relaxed our threshold for hit selection. To improve power for multiple hypothesis testing across the entire genome, we analyzed 390,375 UK Biobank participants with genome-wide genotypes and known plasma lipids (table S7) to search for variants associated with LDL-C among only our hits (33). We filtered to nonsynonymous protein-coding variants in these hits by a threshold minor allele frequency (>0.001) and minimum statistical significance ($P = 0.000427$; Table 1). For basal cell adhesion molecule (*BCAM*), we found both an association between higher LDL-C and a nonsense variant and bidirectional associations between LDL-C and missense variants, suggesting that this pathway may be tunable. We also found associations between elevated LDL-C and variants in methylsterol monooxygenase 1 (*MSMO1*), chromosome 6 open reading frame 132 (*C6orf132*), hepatocyte nuclear factor 4 alpha (*HNF4A*), and timeless circadian regulator (*TIMELESS*), suggesting that these hits may be functional in the human and warrant further evaluation. The results also suggested that the accessible

Table 1. Association of nonsynonymous variants in CRISPRi screen hits with serum LDL-C in the UK Biobank. BETA indicates the linear regression standardized effect size, and P_BOLT_LMM indicates the linear mixed model *P* value using BOLT-LMM (91).

Gene	Variant rsID	Beta	P_BOLT_LMM	Consequence	Impact
<i>HNF4A</i>	rs1800961	0.0564144	0	missense_variant	Moderate
<i>BCAM</i>	rs28399659	-0.0174111	7.70×10^{-29}	missense_variant	Moderate
<i>BCAM</i>	rs200398713	-0.0803165	1.80×10^{-28}	splice_region_variant,intron_variant	Low
<i>BCAM</i>	rs199922856	-0.342179	6.20×10^{-28}	missense_variant	Moderate
<i>BCAM</i>	rs28399654	0.220592	6.10×10^{-10}	missense_variant	Moderate
<i>BCAM</i>	rs3810141	0.020077	5.50×10^{-7}	stop_gained	High
<i>TIMELESS</i>	rs2291738	0.00388393	0.00014	splice_region_variant,intron_variant	Low
<i>BCAM</i>	rs149302547	-0.147327	0.005	missense_variant	Moderate
<i>BCAM</i>	rs1135062	-0.0213642	0.0074	missense_variant	Moderate
<i>C6orf132</i>	rs55772414	0.0116856	0.013	missense_variant	Moderate
<i>MSMO1</i>	rs142496142	0.0432195	0.015	missense_variant	Moderate

“genomic space” of the CRISPRi and GWAS strategies was only partially overlapping.

Regulators of surface LDLR abundance affect functional uptake of LDL

To validate our screen results, we generated CRISPRi HepG2 cells harboring either of the two top-scoring sgRNAs for 77 of our hits and established controls. We preferentially tested hits with an increase in surface LDLR upon inhibition, as well as those with potentially druggable functions or lacking associated GO terms. Because surface receptor abundance might not necessarily correlate to increased function, we evaluated both LDLR and TFR surface phenotypes alongside LDL uptake (34). This functional assay involved a pulse treatment of exogenous, fluorophore-labeled LDL followed by a similar flow cytometric readout. Last, because knockdowns could also cause growth phenotypes, we assayed the number of cells surviving to FACS analysis as a proxy for viability.

We recapitulated the phenotypes for receptor abundance for at least one of the guides in most of the hits (55 genes, 71% of those tested; table S8). Moreover, for 40 of these genes, both sgRNAs were independently validated, suggesting against an off-target effect. We visualized these hits based on their effects, at single-cell resolution, on LDLR and TFR abundance, the LDLR/TFR ratio, functional LDL uptake, and the number of cells surviving to analysis (Fig. 2 and fig. S3B). In this tissue culture model, most knockdowns had independently validated effects on LDLR abundance and LDL uptake of similar or greater magnitude than the *HMGCR* or *PCSK9* controls.

Knockdown of hits expected to alter cellular cholesterol balance or transcriptionally regulate the LDLR showed directionally consistent effects between LDLR abundance and function (Fig. 2). For genes in the enzymatic pathway of cholesterol metabolism [3-hydroxy-3-methylglutaryl-coenzyme A synthase 1 (*HMGCS1*) and *MSMO1*] (35), this was consistent with activation of sterol regulatory element-binding protein 2 (SREBP2)-mediated *LDLR* transcription. For genes encoding certain transcription factors [hepatocyte nuclear factor 1 homeobox A (*HNF1A*) (36), *HNF4A* (37), one cut homeobox 1 (*ONECUT1*) (38), and zinc finger E-box binding homeobox 1 (*ZEB1*) (39)], this

was consistent with an effect on *LDLR* transcription itself. Knockdowns of solute carrier family 25 member 27 (*SLC25A27*), which encodes a mitochondrial uncoupling protein (40), and adenosine triphosphate (ATP)-binding cassette subfamily A member 4 (*ABCA4*), encoding a known lipid transporter (41), both exhibited reductions in LDLR abundance and function (Fig. 2). These genes could plausibly induce a negative lipid balance, increasing LDL uptake via both LDLR-dependent and LDLR-independent mechanisms.

Targeting of hits that either affected multiple transcriptional pathways or regulated endocytosis showed opposite effects on LDLR abundance and function. Knockdown of tribbles pseudokinase 1 (*TRIB1*), a GWAS hit (30) encoding a pseudokinase that regulates the constitutive photomorphogenic (COP1) E3 ligase (42) and affects multiple transcription factors (43), showed this phenotype. In the mouse, *TRIB1* overexpression lowers serum cholesterol, whereas the knockout has the opposite effect (44, 45), consistent with our results. Knockdown of adaptor-related protein complex 2 subunit mu 1 (*AP2M1*), a TFR screen hit that encodes an adaptor protein required for endocytosis (46), was similar, consistent with an accumulation of nonfunctional receptors at the cell surface. This phenotype, although specific to the LDLR, was also seen with knockdown of *BCAM*, which encodes a membrane cell adhesion molecule (47) identified by GWAS (32), and transmembrane protein 217 (*TMEM217*), which encodes an uncharacterized transmembrane protein (Fig. 2 and fig. S4). This suggested that these proteins could have a similar endocytosis adaptor function specific for the LDLR, akin to *LDLRAP1* (48), in which mutations cause a recessive form of FH.

Pharmacologic inhibition of clinically relevant pathways provides mechanistic insight into putative LDLR regulators

We next used pharmacologic approaches to perturb specific pathways of LDLR regulation. We hypothesized that hits might alter cholesterol metabolism, LDLR recycling, or a yet unspecified pathway. By combining CRISPRi knockdown with either a statin to inhibit endogenous cholesterol biosynthesis (21) or a *PCSK9* inhibitor to arrest LDLR lysosomal degradation (24) and assessing the combined effect, we inferred mechanistic information about the target

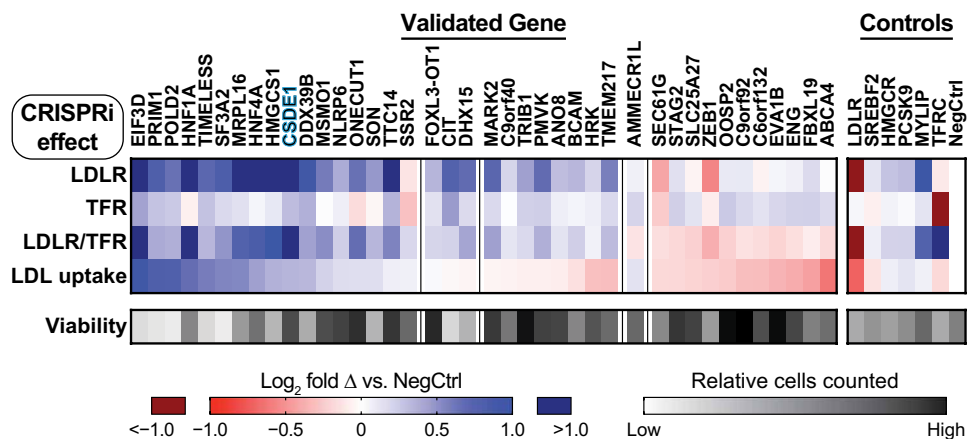


Fig. 2. Validation of LDLR CRISPRi hits. Heatmap showing receptor abundance (LDLR, TFR, and LDLR/TFR ratio) and function (LDL uptake) for dCas9-KRAB HepG2 cells transduced with sgRNA targeting the indicated gene, analyzed by flow cytometry. Hits are grouped according to directional effect on LDLR abundance, and then within groups, by effect on LDL uptake (with uptake from *FOXL3-OT1*, *CIT*, and *DHX15* sgRNAs not significantly different, at $P > 0.05$, from negative control sgRNA). *CSDE1* is highlighted in blue. Control sgRNAs are shown at the right. Readouts show \log_2 fold change (\log_2FC) compared to transduction with negative control sgRNA and represent the weighted average of the effects from both sgRNAs targeting each gene. Viability indicates the relative number of cells surviving to flow cytometry in the experiments. Functional classification of genes is shown in fig. S3. Note that LDLR/TFR is a separately ascertained value from individual cells and not a derived parameter from aggregate data. Only the hits for which two separate sgRNAs independently validated for receptor expression are shown, defined as $P < 0.05$ via Holm-Sidak-corrected t test. Data represent summary information from three to four independent experiments.

gene. Furthermore, we hypothesized that either additive or potentiating effects between a clinically validated therapy and a hit gene might suggest potential therapeutic targets.

We evaluated the receptor abundance and function phenotypes for 29 of our validated hits in the presence or absence of simvastatin (49) or PF-846, a selective inhibitor of PCSK9 translation (Fig. 3 and table S9) (50). We calculated a synergy score by subtracting the differential effects of CRISPRi knockdown, compared to the control, in the presence of a compound from that with the dimethyl sulfoxide vehicle. A more positive value indicated synergy, and a more negative value indicated antagonism.

After knockdown, regulators of cholesterol biosynthesis [sterol regulatory element-binding transcription factor 2 (*SREBF2*), *HMGCR*, *HMGCS1*, *MSMO1*, and phosphomevalonate kinase (*PMVK*)] showed antagonism with the statin but mild synergy with PCSK9 inhibition (Fig. 3). The antagonism with statins was expected, given that *SREBP2* drives *LDLR* transcription. Because *SREBP2* also induces *PCSK9* expression, knockdown of these genes raises the total PCSK9, explaining both the synergy with PCSK9 inhibition that we observed here and that observed with statins in the clinic (51). The synergy phenotypes for knockdown of mitochondrial ribosomal protein L16 (*MRPL16*), which encodes a structural component of the mitochondrial ribosome (52), mirrored these cholesterol biosynthetic genes (Fig. 3), suggesting that MRP-L16 might play a role in the mitochondrial generation of metabolic precursors to sterol biogenesis. In contrast, *C6orf132* knockdown showed the opposite phenotype: mild synergy with a statin and mild antagonism with PF-846 (Fig. 3). *C6orf132* localizes to the Golgi (53), suggesting that it may function by facilitating LDLR delivery to the cell surface, before any interaction with extracellular PCSK9. For some transcription factors, the synergy phenotypes pointed to their downstream targets. For example,

synergy of *HNF1A* knockdown with a statin (Fig. 3) is consistent with the disruption of HNF1- α -mediated *PCSK9* transcription (54).

Cold shock domain-containing protein E1 regulates the stability of LDLR mRNA

One of the strongest hits, cold shock domain-containing E1 (*CSDE1*), also known as upstream of N-ras (*UNR*), encodes an RNA binding protein with varied regulatory functions (55–57), including mRNA decay (58). Because the *LDLR* 3' untranslated region (3'UTR) consists of adenylate-uridylate (AU)-rich elements (AREs) implicated in mRNA stability (59), we hypothesized that *CSDE1* could mediate the degradation of the *LDLR* transcript, thereby explaining its observed receptor abundance, and synergy phenotypes.

Upon *CSDE1* knockdown in HepG2 cells, we observed increased LDLR abundance under both sterol-replete and sterol-depleted conditions (Fig. 4A). Moreover, we observed progressively higher LDLR amounts with sterol depletion and the

addition of a statin (Fig. 4A and fig. S5, A to C), suggesting that the mechanism of *CSDE1* disruption is at least additive with *SREBP2*-mediated *LDLR* transcription and statin therapy. We reproduced our flow cytometry results in *CSDE1*-depleted cells (fig. S6A) with immunoblots against both total and surface LDLR (fig. S6B), capturing the latter via a cell surface biotinylation assay. HepG2 cells transfected with *CSDE1*-targeting small interfering RNA (siRNA) exhibited similarly increased LDLR abundance (fig. S7A) and LDL uptake (fig. S7B) to the CRISPRi results. siRNA against *CSDE1* increased both *LDLR* transcripts in Huh7 cells (fig. S8) and LDL uptake in primary mouse hepatocytes (1.6-fold increase; $P = 0.0372$; fig. S9A). Similar results were observed in primary mouse hepatocytes using adeno-associated virus serotype 8 (AAV8)-delivered short hairpin RNA (shRNA) against *Csde1*, although these outcomes were not statistically significant ($P = 0.373$; fig. S9B). Together, these observations confirm that the effects of *CSDE1* are not limited to a single cell line.

Returning to our CRISPRi HepG2 system, we generated a combined *CSDE1/LDLR* knockdown cell line harboring sgRNAs against each target (60). As expected, the double knockdown had no additional effect on surface LDLR as compared with the *LDLR* knockdown alone (fig. S10, A and B). However, the double *CSDE1/LDLR* knockdown exhibited a small but significant increase in LDL uptake ($P < 0.0001$) compared with the single *LDLR* knockdown ($CSDE1^{\text{nonLDLR}}$; Fig. 4B and fig. S10, C and D). This LDLR-independent effect constituted about 40% of the total increase in LDL uptake driven by *CSDE1* knockdown in the *LDLR*-sufficient background (compare $CSDE1^{\text{nonLDLR}}$ to total *CSDE1* in pie charts; Fig. 4B and fig. S10C). Both LDLR-dependent ($CSDE1^{\text{LDLR}}$) and LDLR-independent components of *CSDE1*'s effect on LDL uptake were additive with and unaffected by sterol depletion and statin therapy ($SREBP2^{\text{LDLR}}$; Fig. 4B and fig. S10,

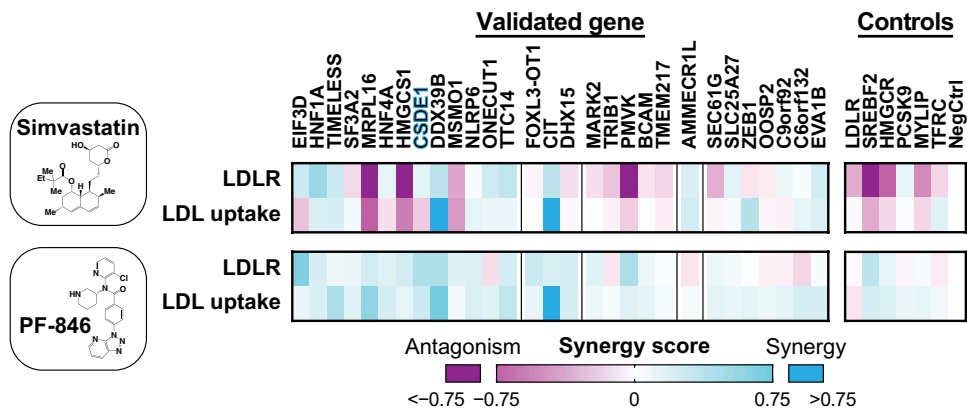


Fig. 3. Synergy of CRISPRi knockdowns with simvastatin or PF-846. Heatmap showing synergy score for knockdowns of indicated genes combined with simvastatin (top) or PF-846 (bottom). Separate LDLR abundance and function (LDL uptake) experiments are shown. Hits are grouped first according to overall effect on LDLR abundance and secondarily by effect on LDL uptake, as in Fig. 2. *CSDE1* is highlighted in blue. Data represent summary information from four independent experiments.

C and D). Furthermore, there was no significant difference in the magnitude of LDL uptake between that driven solely from the LDLR-dependent mechanism of *CSDE1* and sterol depletion and statin ($P = 0.9002$; see pie chart; Fig. 4B). However, in contrast to its equivalent effect on LDL uptake, *CSDE1* knockdown was less effective at up-regulating surface LDLR than *SREBP2* activation (fig. S10, A and B), raising the possibility that *CSDE1* knockdown may also result in a more functional LDLR. Together, these data suggest that the main effect of *CSDE1* on LDL uptake is LDLR dependent, with an additional but smaller LDLR-independent effect also present.

We next observed that overexpression of isoform 1 of *CSDE1*, but not isoforms 2 to 4, reduced surface LDLR in HepG2 cells (Fig. 4C and fig. S11, A to D). Overexpression of all four isoforms of *CSDE1* down-regulated LDLR abundance in the *CSDE1* CRISPRi knockdown cells, although isoform 1 showed the strongest effect (fig. S11, E to I). The opposing directional effects of *CSDE1* knockdown and overexpression suggested that, under physiologic expression conditions, isoform 1 of *CSDE1* is a rate-limiting regulator of the LDLR.

Consistent with our mechanistic hypothesis, we noted more than a twofold increase in steady-state *LDLR* mRNA (Fig. 4D), as well as depleted *CSDE1* (Fig. 4D and fig. S6A), in the *CSDE1* knockdown cells (Fig. 4D). Among control mRNA targets, we also observed significant increases in *MYLIP* and K homology-type splicing regulatory protein (*KHSRP*) mRNA ($P < 0.0001$) but not in *SREBF2*, *PCSK9*, *HMGCR*, or *TFRC* mRNA (Fig. 4D). The gene products of *MYLIP* and *KHSRP* down-regulate the LDLR (27, 61), which is the opposite of our observed phenotype, suggesting that the direct effect of *CSDE1* knockdown on the *LDLR* mRNA predominates in our tissue culture model. To specifically evaluate transcriptional decay, we treated cells with actinomycin D and measured *LDLR* transcripts over time. We observed significantly higher *LDLR* mRNA in the *CSDE1* knockdown cells at all subsequent time points ($P < 0.05$; Fig. 4E). The mRNA half-life, modeled by a single-phase decay equation, was nearly 1.5-fold longer in the *CSDE1* knockdown cells compared to controls ($P = 0.0021$; Fig. 4E). *CSDE1* knockdown had no significant effect on *HMGCR*, *SREBF2*, or *TFRC* mRNA over time ($P > 0.05$; fig. S12, A to C). *CSDE1* knockdown cells exhibited reductions in *PCSK9* and *KHSRP* mRNA at several time points, but the mRNA abundance

over time did not fit a decay equation, suggesting against a *CSDE1*-mediated effect on transcript stability (fig. S12, D and E). By contrast, *CSDE1* knockdown showed a similar extension of transcript half-life on *MYLIP* mRNA as *LDLR* mRNA (fig. S12F), suggesting that *MYLIP* may also be negatively regulated by *CSDE1*. Because the increase in *MYLIP* transcripts seen with *CSDE1* knockdown will down-regulate the LDLR, the targeting of *MYLIP* or its encoded protein, inducible degrader of the LDLR (IDOL), could act synergistically with the targeting of *CSDE1* in lowering LDL-C.

To probe the relationship of *CSDE1* to the *LDLR* 3'UTR, we transiently expressed luciferase constructs (Fig. 4F) under the control of the native *LDLR* promoter in the *CSDE1* knockdown cells.

The luciferase-only constructs showed appropriate physiologic up-regulation by sterols, regardless of *CSDE1* knockdown (Fig. 4G). Constructs fused to the *LDLR* 3'UTR, but not those fused to the *LDLR* coding sequence alone, exhibited increased reporter activity with *CSDE1* knockdown (Fig. 4H). This increase in activity was attenuated by removing the first of four AREs (59, 62) from the 3'UTR (Fig. 4H). Activity of the 3'UTR-fused construct increased further with statin coadministration (Fig. 4I), suggesting that *CSDE1* knockdown may be synergistic with statins, consistent with our prior results (Fig. 3). Together, these findings suggest that, under physiologic conditions, *CSDE1* mediates the decay of the *LDLR* mRNA through its 3'UTR, with the first ARE of the UTR required for its full effect.

Disruption of *CSDE1* up-regulates *Ldlr* mRNA expression and protects from cholesterol loading in zebrafish and mice

We then turned to an in vivo model in zebrafish, because the 3'UTR of its ortholog *ldlra* (XM_005163870.4) is AU rich and contains at least two canonical ARE sequences for mRNA regulation (63). The *ldlra* knockout in zebrafish results in hyperlipidemia and vascular lipid accumulation, and challenging larvae with a high-cholesterol diet is sufficient to increase their overall cholesterol content (64). We used yolk microinjection of a Cas9-ribonucleoprotein (RNP) complex containing redundant guides to achieve near-saturation gene disruption (65), followed with dietary cholesterol supplementation, and evaluated total cholesterol in the larvae (64). Targeting of *csde1* protected against total cholesterol accumulation, with a modest (12%) but significant reduction ($P = 0.0017$) in total cholesterol in 8-day post fertilization (dpf) zebrafish (fig. S13, A to C), without any obvious phenotypic abnormalities (fig. S13, D to F). By contrast, targeting of *ldlra* showed the expected 1.4-fold increase in total larval cholesterol (fig. S13A), consistent with prior studies (64).

We then probed the effect of *Csde1* gene silencing in the mouse as a therapeutic proof of principle, given even greater homology between the 3'UTRs of the murine and human *LDLR* orthologs (66). Using wild-type C57BL/6 mice, we delivered shRNA against *Csde1* (57) or a scramble control via an AAV8 vector. One week after delivery of a moderate dose of AAV8 (3×10^{11} genomes per mouse), we harvested blood and tissue samples from the mice. We found

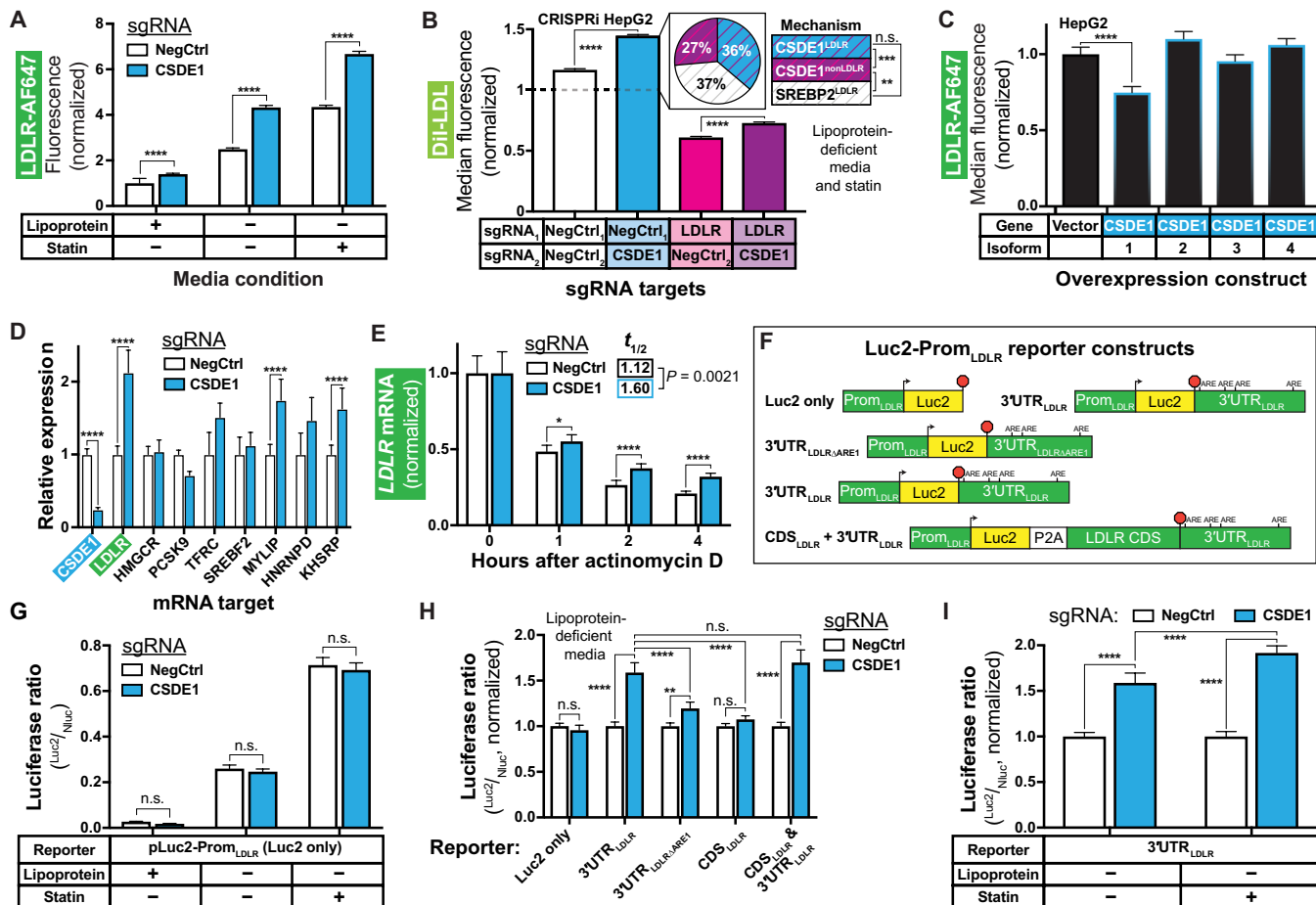


Fig. 4. CSDE1 mediates LDLR mRNA decay. (A) Relative LDLR abundance in CRISPRi HepG2 cells transduced with indicated sgRNAs and grown in the indicated media. (B) Relative LDL uptake in dual-sgRNA CRISPRi HepG2 cells. The pie chart shows the relative contribution of LDLR-dependent (CSDE1^{LDLR}; blue with purple stripes) and LDLR-independent (CSDE1^{nonLDLR}; purple with magenta stripes) CSDE1-mediated mechanisms, as well as SREBP2-mediated mechanisms (SREBP2^{LDLR}; white with gray stripes) to LDL uptake. Data are normalized to the control cells in standard media (dashed line; data shown in fig. S10C). (C) Relative LDLR abundance in HepG2 cells overexpressing the indicated CSDE1 isoforms. (D) Relative expression of the indicated mRNA targets in CRISPRi cells under sterol-depleted conditions. (E) Relative expression of *LDLR* mRNA in CRISPRi cells after arrest of transcription with actinomycin D. Data normalized at $T=0$ within the sgRNA evaluated to illustrate the change in time, and thus, no comparison can be made at $T=0$. $t_{1/2}$ indicates data fit to a one-stage exponential decay equation and analyzed by extra sum-of-squares F test. (F) Schematics (not to scale) of Luc2-Prom_{LDLR} reporter constructs, illustrating *LDLR* promoter, start site (arrowhead), P2A ribosomal skipping sequence, ARES in 3'UTR, stop codon (red octagon), and indicated regions of the *LDLR* gene. (G to I) Ratiometric luciferase outputs of CRISPRi cells transfected with indicated reporters. "Luc2 only" used in (G), all constructs used in (H), and "3'UTR_{LDLR}" used in (I). Outputs normalized to negative control in (H) and (I). (A to I) Data represent summary information from three to four independent experiments. n.s., $P \geq 0.05$; * $P < 0.05$; ** $P < 0.01$; *** $P < 0.001$; **** $P < 0.0001$.

that, compared to scramble controls, the *Csde1*-targeted mice exhibited about 30% reduction in hepatic *Csde1* mRNA and about 1.8-fold increase in hepatic *Ldlr* mRNA (Fig. 5A), no gross histologic abnormalities in the liver (fig. S14, A to D), and robust expression of the enhanced green fluorescent protein (eGFP) reporter encoded by the AAV8 vector (fig. S14, E to L). With *Csde1* knockdown, we also observed a corresponding reduction in hepatic CSDE1 protein (Fig. 5B). However, steady-state hepatic LDLR protein amounts were not significantly different ($P = 0.826$; Fig. 5B). We also saw no differences in the hepatic lipoprotein receptors LDLR-related protein 1 (LRP1) or scavenger receptor class B type 1 (SR-B1; Fig. 5B), hepatic PCSK9 protein (Fig. 5B and fig. S14, E' to L'), the appearance or behavior of the mice, plasma alanine or aspartate aminotransferase activity (fig. S15A), or total hepatic bile acids (fig. S15B).

These observations suggested a lack of toxicity of either the *Csde1* shRNA or the gene knockdown.

To evaluate the functional effect of *Csde1* gene disruption, we turned to C57BL/6 mice on a Western-type (high-fat, high-cholesterol) diet. We obtained baseline plasma samples on this diet and delivered a moderate dose (3×10^{11} genomes per mouse) of the AAV8-shRNA targeting either *Csde1*, *Pcsk9*, or a scramble control. Two weeks after transduction, we reassessed total plasma cholesterol. We observed a significant decrease, compared to baseline, only for the mice transduced with *Csde1*-targeting shRNA (21% reduction; $P = 0.0027$; Fig. 5C). The decrease observed with *Pcsk9*-targeting shRNA fell just outside our prespecified cutoff for significance ($P = 0.0592$). Lipoprotein fractionation of the posttransduction samples (fig. S16A) revealed a 39% reduction in cholesterol in the LDL-containing fractions

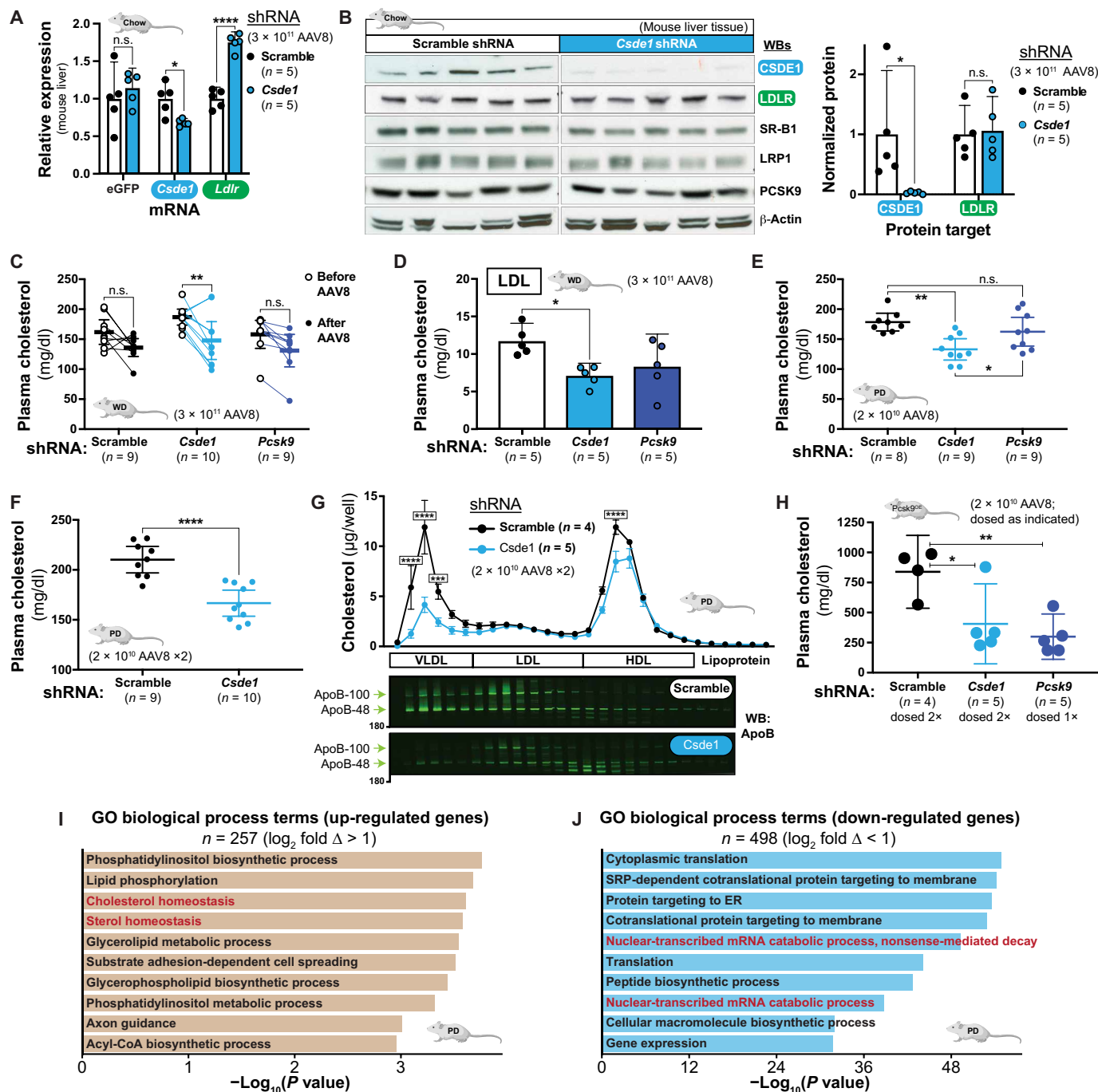


Fig. 5. CSDE1 disruption up-regulates *Ldlr* mRNA and LDLR function in mice. (A) Relative expression of hepatic eGFP, *Csd1*, and *Ldlr* transcripts in chow-fed mice transduced with the indicated moderate-dose AAV8-shRNA. Matched two-way ANOVA with Holm-Sidak multiple comparisons test is shown. (B) Immunoblots of liver extracts from mice in (A). Each lane represents an individual mouse. Quantification of protein, normalized to loading control, is shown at the right. Unpaired t tests are shown. (C) Mean plasma cholesterol concentrations of Western diet-fed (WD) mice before and 2 weeks after transduction with moderate-dose AAV8-shRNA. Matched two-way ANOVA with Sidak multiple comparisons test is shown. (D) Mean LDL-C concentrations, fractionated by gel filtration, from individual mice from (C). (E) Mean plasma cholesterol concentrations of Paigen diet-fed (PD) mice 2 weeks after transduction with low-dose AAV8-shRNA. (F) Mean plasma cholesterol concentration of mice in (E) 2 weeks after transduction with a second low-dose AAV8-shRNA. (G) Top: Mean cholesterol concentrations of fractions collected from gel filtration of plasma from individual mice in (F). Bottom: Immunoblots of fractions from representative mice against ApoB are shown. Note that fractions shown begin with the elution front from the size exclusion column. Two-way ANOVA with Sidak's multiple comparisons test is shown to illustrate comparison between treatment arms within a given fraction. Error bars indicate SEM. (H) Mean plasma cholesterol concentrations of *Pcsk9*-D377Y-overexpressing and Paigen diet-fed mice 2 weeks after transduction with a second dose of low-dose AAV8-shRNA (8 weeks after first dose, for singly dosed mice). Note that *Pcsk9*-targeted mice were only given the first dose of AAV8. (I and J) Leading up-regulated (I) and down-regulated (J) biological process GO terms in the differentially expressed genes (adjusted $P < 0.05$, $\log_2FC > |1|$) in *Csd1* knockdown mice on the Paigen diet. (A to J) n.s., $P \geq 0.05$; * $P < 0.05$; ** $P < 0.01$; *** $P < 0.001$; **** $P < 0.0001$.

between the *Csde1* knockdown mice and scramble controls ($P = 0.0272$; Fig. 5D) but no difference in the very-low-density lipoprotein (VLDL) or high-density lipoprotein (HDL) fractions (fig. S16, B and C). Consistent with prior literature (23), we observed an increase in total hepatic LDLR protein with *Pcsk9* knockdown (fig. S16D), but as with chow-fed mice, we observed no differences in the histologic appearance of the liver (fig. S17, A to D) or in the levels of hepatic LDLR protein between the scramble control and *Csde1* knockdowns ($P = 0.744$; figs. S16D and S17, E' to L').

To better assess the effects on non-HDL cholesterol, we also studied C57BL/6 mice on the atherogenic, cholate-rich Paigen diet (67, 68). Here, we delivered low-dose (2×10^{10} genomes per mouse) AAV8-shRNA targeting either *Csde1*, *Pcsk9*, or a scramble control. Two weeks later, we observed a 25% reduction in fasting plasma cholesterol in the *Csde1* knockdown mice, which exceeded the effect of *Pcsk9* knockdown ($P = 0.0497$; Fig. 5E). We then redosed the *Csde1* and scramble AAV8-shRNA and, 2 weeks later, observed an even stronger phenotype (Fig. 5F). Despite the lower dose of AAV8 delivered, we observed the expected reduction in *Csde1* mRNA and an increase in *Ldlr* mRNA in the livers of the *Csde1*-targeted mice (fig. S18A). Lipoprotein fractionation of the mouse plasma showed that *Csde1* knockdown most strongly affected the VLDL-containing fractions (Fig. 5G), with immunoblots confirming a reduction in both apolipoprotein B100 (ApoB-100) and ApoB-48, consistent with an increase in function of the murine LDLR on a cholate-rich dietary background (69, 70). As with the chow-fed mice, we observed no clear difference in the steady-state amount of LDLR protein in the liver (fig. S18B) nor did we observe hepatotoxicity from the *Csde1*-targeting shRNA (fig. S18C).

Last, we also used a murine PCSK9 overexpression model to further assess the effects on atherogenic lipoproteins in a LDLR-depleted system. Again, using C57BL/6 mice on the atherogenic, cholate-rich diet, we simultaneously delivered low-dose AAV8-*Pcsk9*-D377Y with low-dose AAV8-shRNA targeting either *Csde1*, *Pcsk9*, or a scramble control. We purposefully chose the submaximal dose (2×10^{10} genomes per mouse) for AAV8-*Pcsk9*-D377Y delivery (71) to reduce, but not completely ablate, the LDLR, given our hypothesis that CSDE1's effects on cholesterol are LDLR dependent. Two weeks after AAV8 delivery, we observed a marked reduction (73%; $P = 0.0351$) in total plasma cholesterol in the shRNA-*Pcsk9*-treated mice and a similar (57%) but nonsignificant ($P = 0.1013$) reduction in the shRNA-*Csde1*-treated mice, both when compared to the scramble controls (fig. S19). We therefore redosed the mice in the *Csde1* and scramble treatment arms with the corresponding AAV8. Two weeks after this second dose, which was 8 weeks after the first dose, we again measured total plasma cholesterol and observed significant reductions for the *Csde1* (52%; $P = 0.0194$) and the singly dosed *Pcsk9* (64%; $P = 0.0052$) knockdowns, both in comparison to the scramble controls (Fig. 5H). Together, the results of these four mouse models suggest that hepatic CSDE1 down-regulates *Ldlr* mRNA expression and reduces clearance of non-HDL in vivo.

The in vivo effect of hepatic CSDE1 silencing on the mouse transcriptome

To gain further insight into the role of hepatic CSDE1, we performed bulk RNA sequencing (RNA-seq) on the liver tissue in the model with the strongest phenotype, the Paigen diet. We compared the *Csde1* knockdown to control (scramble) mice (fig. S20, A to C) using the mice with the highest transcript counts of a vector-delivered

eGFP reporter to control for variations in transduction efficiency. Because mice on the Paigen diet received a lower dose of AAV8 vector, we also filtered our results for the differentially expressed transcripts in the control mice at the extremes of eGFP expression to control for the effects of viral transduction alone. As expected, we found higher *Ldlr* expression in the *Csde1* knockdown mice [\log_2 fold change (\log_2FC) = 0.43, $P = 0.0029$; table S10]. Consistent with our mechanistic hypothesis, GO enrichment analysis of the top differentially expressed genes ($\log_2FC > |1|$, 745 genes in total) revealed up-regulation of genes involved in cholesterol homeostasis ($P = 2.5 \times 10^{-4}$; Fig. 5I, fig. S20D, and table S11) and down-regulation of genes involved in mRNA catabolic processes ($P = 4.9 \times 10^{-50}$; Fig. 5J and table S11) or encoding RNA binding functions ($P = 4.6 \times 10^{-29}$; fig. S20E and table S11). To remove the confounding effects of liver inflammation and steatosis induced by the cholate-containing diet (68), we repeated the bulk RNA-seq in chow-fed mice (fig. S21, A to C). Compared to the mice on the Paigen diet, we observed fewer differentially expressed genes in the chow-fed *Csde1* knockdowns (43 genes in total, any \log_2FC ; fig. S21, B and C, and table S12), consistent with less homeostatic perturbation. In agreement with the results from the Paigen diet model, we observed a positive enrichment for genes promoting mRNA stability ($P = 4.9 \times 10^{-4}$; fig. S21D and table S13) and a negative enrichment for genes encoding RNA binding functions ($P = 2.7 \times 10^{-3}$; fig. S21E and table S13).

DISCUSSION

Since their introduction, statins, which up-regulate the LDLR, have become a major public health success, and with the discovery of PCSK9 and the therapeutic antibodies targeting it, patients can safely reach much lower LDL than is achievable by statins alone (72). However, we may be able to push further on this LDL-LDLR axis to achieve greater clinical benefits.

In this study, we modeled a clinically relevant phenotype of LDLR abundance and function, complementing the independent investigations of other groups (73, 74). When synthesizing our screening and validation data together with large-scale genomics and additional pharmacologic perturbations, we produced an exploratory map of potential regulatory mechanisms for the LDLR (fig. S22). These data represent promising targets and also pathways likely to be affected by therapies already in use in the clinic.

We have shown that CSDE1 regulates LDLR abundance in HepG2 cells by promoting *LDLR* mRNA decay via its 3'UTR. These data lay in concert with CSDE1's destabilizing effects on other transcripts, such as *c-Fos* (58). We have also shown that in vivo knockdown of *Csde1* up-regulates hepatic *Ldlr* mRNA expression and improves atherogenic lipid profiles in mice. This mimics the effect of deleting the 3'UTR in vivo (75) and phenocopies a human variant with a large deletion in the *LDLR* 3'UTR, the only gain-of-function *LDLR* mutation identified that markedly reduces LDL-C (76). It is notable that several small molecules, including triciribine (62) and berberine (66, 77), have stabilizing effects on *LDLR* mRNA, although whether their mechanisms directly involve CSDE1 remains to be elucidated. The magnitude of LDLR up-regulation imparted by CSDE1 knockdown mirrored or exceeded that of *HMGCR* and *PCSK9* in both tissue culture and mouse models, suggesting that a high-fidelity approach targeting CSDE1-mediated *LDLR* mRNA decay in the clinic could have similar effects. In addition, our mechanistic data suggest that targeting CSDE1 could be at least additive with the use of statins.

Although after *CSDE1* knockdown we observed an increase in hepatic LDLR protein in our human tissue culture models, we observed no change in total hepatic LDLR protein in our mouse models despite a reduction in LDLR-cleared lipoproteins. Whether this difference between our models reflects hepatocyte physiology within an intact organism or instead a species-specific difference between the HDL-predominant mouse (69, 70) and the LDL-predominant human remains to be determined. Our data are consistent with metabolic labeling experiments demonstrating the homeostatic defense of steady-state hepatic LDLR in the mouse in response to cholesterol loading conditions and altered *LDLR* transcription (78). Our data are also consistent with mouse experiments that markedly perturb *Ldlr* mRNA but have comparatively muted effects on LDLR protein (66, 79). We hypothesize that inhibition of *CSDE1* protects *LDLR* mRNA from *CSDE1*-mediated decay, up-regulates LDLR synthesis, and induces in vivo homeostatic mechanisms that together increase LDLR function but maintain steady-state LDLR abundance in the mouse. The nature of these mechanisms will be important to uncover. Intriguingly, our tissue culture data showed that, compared to a statin, disrupting *CSDE1* had a disproportionately larger effect on LDL uptake than surface LDLR amounts, supporting the possibility that *CSDE1* could also affect LDLR function, in addition to its abundance. Furthermore, these data also showed that *CSDE1* knockdown also increased *MYLIP* transcripts. Because the gene product of *MYLIP*, IDOL, induces posttranslational degradation of the LDLR, this effect might help explain our in vivo findings. In support of this possibility, the transcriptomic profiling of the chow-fed *Csde1* knockdown mice revealed a negative enrichment in genes encoding ubiquitin ligase binding ($P = 5.9 \times 10^{-3}$; fig. S21D and table S13), suggesting that ubiquitin-dependent regulators such as IDOL may be perturbed. Given our observation of increased LDL uptake with *CSDE1* knockdown in the *LDLR*-deficient background, a separate LDLR-independent effect of *CSDE1* on lipoproteins may also contribute. Further work is needed to investigate the potential contributions of these and other mechanisms, such as increased endocytic turnover of existing LDLR and altered synthesis and secretion of non-HDLs.

The degree to which *CSDE1* inhibition affects other transcripts or other tissues (57, 80) also remains an important question. As an RNA chaperone, *CSDE1* can have a variety of effects, from mRNA stabilization (56) to the promotion or inhibition of translation (81–83), dependent on the identity of the RNA it binds and the cofactors with which it interacts. Intriguingly, although *CSDE1* was found to bind biotinylated *LDLR* 3'UTR transcripts in HepG2 cell lysates (61), cross-linking immunoprecipitation approaches in both mouse brain and melanoma cells failed to identify *LDLR* mRNA as a *CSDE1* binding partner (84, 85). This suggests that the *CSDE1*-*LDLR* interaction is context dependent. Advances in liver-specific delivery of gene silencing agents (15, 86), gene editing technologies (87), and small molecules (88) offer the possibility that selectively targeting hepatic *CSDE1* for cholesterol lowering could avoid systemic toxicities.

We acknowledge several limitations in our study. First, outside of *CSDE1*, the validation of gene targets affecting both LDLR abundance and function is limited to a single cell line. In addition, of our validated hits in tissue culture, we only confirmed *CSDE1* in an in vivo mammalian model. Third, the fundamental differences in lipoprotein metabolism in the mouse may limit the translation of our conclusions surrounding *CSDE1* to humans (69, 70). Last, we have not directly assessed the effects of *CSDE1* disruption in non-hepatic tissues.

Nevertheless, we observed no ill effects from *CSDE1* disruption in either our tissue culture or in vivo models, and our transcriptional profiling suggests only a small number (43) of differentially affected transcripts under normal feeding conditions. This suggests that potential toxicities of hepatic *CSDE1* disruption may be low, which will be important to confirm in future studies that pursue *CSDE1* as a therapeutic target for cholesterol lowering. Given that *CSDE1* has such varied effects on other transcripts, further mechanistic dissection of the hepatic *CSDE1*-*LDLR* interaction could identify what makes this relationship unique and guide a potential therapeutic strategy. Our transcriptomic analyses may guide subsequent investigations of both possible toxicities and mechanistic details of hepatic *CSDE1* disruption. Combination therapies targeting interconnected pathways to disease can provide increased benefits without inducing extreme side effects, with angiotensin receptor blockade and neprilysin inhibition in heart failure a prominent clinical example (89). To the extent that hepatic *CSDE1* uses specific factors to down-regulate *LDLR* mRNA, simultaneous tissue-specific drugging of both *CSDE1* and these factors could widen the overall therapeutic window.

In summary, we leveraged a clinically relevant phenotype in an unbiased, genome-wide forward genetic screen to identify a panel of previously unrecognized regulators of the LDLR. Together, our mechanistic experiments in tissue culture and physiologic models in mice suggest that *CSDE1* regulates hepatic LDLR function by promoting *LDLR* mRNA decay and may be a potential therapeutic target for heart disease.

MATERIALS AND METHODS

Study design

We designed the study as a discovery biology experiment to identify new regulators of the LDLR. We used an established tissue culture model, HepG2 cells, to evaluate for LDLR regulation. We used wild-type zebrafish (Ekwill) and wild-type mice (C57BL/6) to validate the contribution of our top hit, *CSDE1*, to LDLR regulation in vivo. We evaluated sufficient cells for the LDLR and TFR screens to provide adequate coverage for transduction and downstream sequencing of each sgRNA in the genome-wide library. Sample sizes for animal experiments were estimated to provide 80% power (two-tailed $\alpha = 0.05$) for a 25% difference in cholesterol compared to controls, based on effects in these models in the existing literature. The numbers of animals used in each experiment are noted in the figures and manuscript. Unless otherwise noted, all in vitro data are representative of multiple (≥ 3) biological replicates to ensure robust outcomes. Experimental and control arms were randomly assigned at the outset of the experiment, with no exclusion criteria predefined and animal samples selected randomly for analyses requiring only a subset of the treatment arm. Experiments were not performed in a blinded fashion. All animal studies were performed in accordance with institutional animal care and use committee-approved protocols at the University of California, San Francisco and the National Institutes of Health Guide for the Care and Use of Laboratory Animals. Reporting of the animal studies is in compliance with Animal Research: Reporting of In Vivo Experiments (ARRIVE) guidelines 2.0 listed in the Enhancing the QUALITY and Transparency Of health Research (EQUATOR) Network library.

Generation of CRISPRi cell lines

All cell lines were transduced using virus-containing supernatant in the presence of polybrene (8 $\mu\text{g}/\text{ml}$; MilliporeSigma). HepG2 cells

expressing dCas9-KRAB were derived by transduction with lentivirus harboring SFFV-dCas9-BFP-KRAB, followed by two rounds of FACS for blue fluorescent protein (BFP)-positive cells on a Becton Dickinson (BD) FACSaria II. dCas9-KRAB HepG2 with individual targeting sgRNAs were derived by transduction with lentivirus harboring the desired sgRNA, followed by 48 hours of puromycin selection (2 µg/ml; InvivoGen), before experiments.

Quantitative reverse transcription polymerase chain reaction

dCas9-KRAB HepG2 cells stably expressing an appropriate sgRNA were harvested and lysed, and total RNA was extracted via the RNeasy Mini Kit (QIAGEN). RNA was converted into complementary DNA (cDNA) using the qScript cDNA SuperMix (QuantaBio) following the manufacturer's instructions. Quantitative reverse transcription polymerase chain reaction (RT-qPCR) was performed against indicated targets with PrimeTime qPCR primers (Integrated DNA Technologies) using the SYBR Select Master Mix (Thermo Fisher Scientific) according to the manufacturer's instructions on a CFX96 Touch Real-Time PCR Detection System (Bio-Rad). Fold changes were calculated using $\Delta\Delta C_t$ analysis, normalizing each sample to *B2M* controls, using CFX Maestro software (Bio-Rad). RNA extracted from mouse liver from in vivo experiments was processed similarly but with additional *B2m*, *Actb*, and *Gapdh* housekeeping controls.

Genome-wide CRISPRi screen

The screen was conducted similarly to prior descriptions (12–14). About 200×10^6 dCas9-KRAB HepG2 cells were transduced with hCRISPRi-v2 top five sgRNAs/gene lentivirus at a multiplicity of infection of ~0.5, and with polybrene (8 µg/ml), on day 1. Cells were grown on 15-cm dishes, subdivided into four replicates immediately upon transduction (biological duplicate for each screen), and re-seeded every 3 to 4 days as necessary to avoid overconfluence. Cells were selected with puromycin (2 mg/ml) from days 2 to 6. On day 5, cells for the LDLR sort were placed in Dulbecco's modified Eagle medium (DMEM) with 5% lipoprotein-deficient serum (LPDS). On day 7, about 50×10^6 cells from two replicates were live-dead stained and sorted for LDLR as described in Supplementary Materials and Methods and then two-way sorted on a BD FACSaria II for the top and bottom 33% by LDLR abundance. Cells were spun down, washed in phosphate-buffered saline (PBS), and frozen at -80°C . On day 8, the sort was repeated except in one replicate, and cells were stained for TFR instead of LDLR and then sorted as per above. Genomic DNA was isolated using a NucleoSpin Blood DNA extraction kit (Macherey-Nagel). The sgRNA-containing region was PCR-amplified with NEBNext Ultra II Q5 MasterMix (New England Biolabs), acrylamide gel-purified, and size-selected by solid phase reversible immobilization (SPRI) beads (Beckman Coulter), all as previously described, before sequencing on an Illumina HiSeq 4000.

Human genomic analysis

Protein-coding variants for hits validated with individual sgRNAs were assayed in the UK Biobank (90) for associations with LDL-C. In the setting of a statin medication, LDL-C was divided by 0.7 as done previously (31). Genotyping and imputation were performed in the UK Biobank as previously described (33), and nonsynonymous protein-coding variants with minor allele frequencies greater than 0.001 were considered. Efficient linear mixed models adjusting for age, sex, genotyping array, and principal components of ancestry were used,

using BOLT-LMM (91). Statistical significance was assigned at $\alpha = 0.05/117 = 0.000427$ to account for multiple hypothesis testing.

Overexpression experiments

HepG2 or engineered dCas9-HepG2 cell lines were seeded into 96-well plates at 5×10^4 cells per well in HepG2 growth medium. After 24 hours, cells were washed and changed into low-glucose DMEM with 5% LPDS. Each well was transfected with 100 ng of the appropriate CSDE1 overexpression construct, or vector control, in a total of 10 µl of Opti-MEM (Thermo Fisher Scientific) using Lipofectamine 3000 (Thermo Fisher Scientific) according to the manufacturer's instructions. Cells were incubated at 37°C with 5% CO_2 for 72 hours and then harvested for LDLR expression analysis as described in Supplementary Materials and Methods.

mRNA decay experiments

Engineered dCas9-HepG2 cell lines harboring appropriate sgRNAs were seeded into 12-well plates at 5×10^5 cells per well in HepG2 growth medium. After 24 hours, cells were washed and changed into sterol-depleting media (low-glucose DMEM with 5% LPDS) supplemented with 6 µM simvastatin. After an additional 24 hours, actinomycin D (MilliporeSigma) was added at 5 µg/ml, and cells were harvested at the indicated time points.

siRNA and AAV8-shRNA knockdowns in tissue culture

Appropriate cell types were transfected with Silencer Select siRNA (Thermo Fisher Scientific) against *CSDE1* (assay ID s15373) or control (negative control no. 1) at a final concentration of 25 µM with RNAiMAX (Thermo Fisher Scientific) according to the manufacturer's instructions. For HepG2 cells, reverse siRNA transfections were performed, and for Huh7 cells and primary hepatocytes, forward transfections were performed. For primary hepatocytes, the transfection agent was removed and replaced with fresh media after 4 hours. For AAV8-delivered shRNA, primary mouse hepatocytes were transduced with custom-generated AAV8 (Vector Biolabs) at about 1×10^6 genomes per cell with 4 mM polybrene. Cells were incubated at 37°C with 5% CO_2 for 72 hours, with daily media changes for primary hepatocytes, before downstream analyses (RT-qPCR, LDLR abundance, and LDL uptake as described above and in Supplementary Materials and Methods).

Dual-luciferase assays

Engineered dCas9-HepG2 cells were seeded into opaque white 96-well plates, at 2.2×10^4 cells per well, in 100 µl of growth medium the day before transfection. On the day of transfection, medium was replaced or changed to sterol-depleted medium (low-glucose DMEM with 5% LPDS) with or without 6 µM simvastatin as appropriate. Each well was transfected with 100 ng of Luc2-Prom_{LDLR}-based construct and 1 ng of secreted nanoluciferase control construct (pSS-NLuc) in a total of 10 µl of Opti-MEM using Lipofectamine 3000 according to the manufacturer's instructions. Six replicates were transfected per construct per experiment. After 48 hours at 37°C and 5% CO_2 , 10 µl of medium was removed from each plate and aliquoted into a separate 384-well plate. Firefly luciferase activity was evaluated in the plates containing the cells by adding an equal volume of a 2× firefly lytic assay buffer [100 mM tris-HCl (pH 7.7), 50 mM NaCl, 2 mM MgCl_2 , 0.17% Triton X-100, 10 mM dithiothreitol, 0.4 mM coenzyme A, 0.3 mM ATP, and luciferin (0.28 mg/ml) (GoldBio)] (92). Nanoluciferase activity was evaluated from the conditioned

medium using a nonlytic 2× coelenterazine (GoldBio) reagent as previously described (93, 94). Raw luminescence was obtained on a Spark plate reader (Tecan) with 1-s integration time. Readout of firefly luciferase in each well was normalized to the corresponding secreted nanoluciferase control, and data were visually inspected and cleaned to remove values from poorly transfected wells [formally defined by Robust regression and OUTlier removal (ROUT) = 1%] during analysis.

Zebrafish handling, maintenance, and Cas9-RNP knockdowns

All zebrafish studies were performed as previously described (65) with minor modifications. Briefly, wild-type zebrafish embryos were injected at the one-cell stage with Cas9-RNP complexes and raised at 28°C. Cas9-RNP complexes were prepared as previously described (65) using custom oligonucleotides against the indicated targets (Elim Biopharmaceuticals). Targeting of tyrosinase, which results in larval albinism, was used as an injection control. Larvae were fed a high-cholesterol diet (64) of Golden Pearls (5 to 50 µm; Brine Shrimp Direct) supplemented [4% (w/w)] with cholesterol (MilliporeSigma) three times daily from 4 dpf, fasted on 7 dpf to clear intestinal cholesterol, and harvested at 8 dpf. Larvae were collected, extensively washed, anesthetized in tricaine, and collected in groups of 10 per sample before storage at –80°C.

Cholesterol analysis of zebrafish homogenates

Total cholesterol was analyzed as previously described (64) with minor modifications. Briefly, frozen larvae were homogenized in PBS with a plastic pestle and then clarified at 18,000g for 15 min. Supernatants were recovered, and total protein content was analyzed by bicinchoninic acid assay. Homogenates were then analyzed, in duplicate, at the appropriate dilution (typically 1:12 in PBS) for total cholesterol content using a commercial fluorometric assay (Cayman Chemical). Fluorescence outputs were measured on a Tecan Spark plate reader, and cholesterol concentrations were interpolated from a regression line calculated from a standard curve. Cholesterol was normalized to total protein content for analysis and subsequently to the scramble control for comparison between experiments.

Mouse handling, maintenance, and shRNA knockdowns

Eight- to 10-week-old male C57BL/6 mice (the Jackson Laboratory) were maintained on a normal chow diet and then placed on the Western diet (0.15% cholesterol and 21% fat; D12079Bi, Research Diets) or atherogenic “Paigen” diet (1.25% cholesterol, 15% fat, and 0.5% cholate; D12336i, Research Diets) (67) at the beginning of the appropriate experiment (week 0). After 2 to 4 weeks on the appropriate diet, AAV8-packaged expression vector encoding *Pcsk9-D377Y* or eGFP or AAV8-packaged shRNA against mouse *Csde1* (NM_144901), *Pcsk9* (NM_153565), or scramble control (Vector Biolabs) was diluted in sterile PBS to a concentration of either 2×10^{11} (low dose) or 3×10^{12} (moderate dose) genomes/ml. One hundred microliters of diluted AAV8 (2×10^{10} or 3×10^{11} genomes per mouse) harboring the appropriate construct shRNA was administered to each mouse via tail vein injection. Two weeks after AAV8 injection, mice were fasted overnight and then underwent blood sampling via submandibular vein puncture. About 50 µl of blood was collected into an EDTA-coated tube and centrifuged at 2000g for 10 min at 4°C, and the plasma was recovered and stored at –20°C until further analysis. Total plasma cholesterol, after about 1:200 to 1:400 dilution in

assay buffer or 1:4000 dilution for *Pcsk9-D377Y*-boosted mice, was evaluated by commercial fluorometric cholesterol assay (Cayman Chemical) according to the manufacturer’s instructions. Mouse plasma was evaluated for alanine and aspartate aminotransferase activity using commercial assays (Cayman Chemical) according to the manufacturer’s instructions. For mice on the Paigen diet, 6 weeks after initial AAV8 injection, mice from the same exposure arm were redosed with AAV8-shRNA targeting either *Csde1* or scramble control. At the time of sacrifice, the mice were again fasted overnight and then euthanized after CO₂ narcosis followed by cervical dislocation. The abdominal cavity was opened with a ventral midline incision, the inferior vena cava was cannulated, and plasma was collected as described above. The liver and vasculature were perfused with PBS, and the samples of the liver were harvested. Tissue samples for RNA evaluation were placed in TRIzol (Thermo Fisher Scientific), and those for protein analysis were flash-frozen in liquid N₂ and stored at –80°C.

RNA-seq library preparation

Total RNA was extracted from frozen liver samples using the QIAGEN RNeasy Plus Universal mini kit following the manufacturer’s instructions (QIAGEN). RNA samples were quantified using a Qubit 2.0 fluorometer (Thermo Fisher Scientific), and RNA integrity was checked using Agilent TapeStation 4200 (Agilent Technologies). Purified RNA was used for mouse RT-qPCR experiments as described above. RNA-seq libraries were prepared via polyadenylate selection using the NEBNext Ultra RNA Library Prep Kit for Illumina using the manufacturer’s instructions (New England Biolabs). Briefly, mRNAs were initially enriched with oligo(dT) beads. Enriched mRNAs were fragmented for 15 min at 94°C. First-strand and second-strand cDNAs were subsequently synthesized. cDNA fragments were end-repaired and adenylated at 3’ ends, and universal adapters were ligated to cDNA fragments, followed by index addition and library enrichment by PCR with limited cycles. The sequencing library was validated on the Agilent TapeStation (Agilent) and quantified by using a Qubit 2.0 fluorometer (Invitrogen) as well as by qPCR (KAPA Biosystems). The sequencing libraries were clustered on a single lane of a flow cell. After clustering, the flow cell was loaded on the Illumina HiSeq instrument (4000 or equivalent) according to the manufacturer’s instructions. The samples were sequenced using a 2 × 150–base pair paired-end configuration. Image analysis and base calling were conducted by the HiSeq Control Software. Raw sequence data (.bcl files) generated from Illumina HiSeq were converted into fastq files and demultiplexed using Illumina’s bcl2fastq 2.17 software. One mismatch was allowed for index sequence identification. RNA library preparation and sequencing were conducted by GENEWIZ LLC.

RNA-seq analysis

All raw sequencing data underwent quality control checks with FastQC (v0.11.8). Reads were mapped to the mm10 mouse reference genome using Rsubread (v2.4.3) and assigned to Ensembl gene IDs. Ensembl gene IDs were then mapped to org.Mm.eg.db (v3.12.0) gene symbols using AnnotationDBI (v1.52.0). Gene expression was quantified using raw counts, and differential expression gene testing was performed on the scramble-shRNA samples comparing the groups ($n = 3$ in each group) at the highest and lowest amounts of raw eGFP expression in the Paigen diet model with EdgeR (v3.32.1) (95, 96) using the glmQLFit method and default settings (97). Statistical significance was set at 5% false discovery rate (Benjamini-Hochberg).

Differential expression gene testing was then performed on the *Csde1* shRNA and scramble shRNA at the highest amounts of eGFP expression with the overlap of differentially expressed genes identified between these two analyses subsequently removed. Functional enrichment gene set analysis for GO terms was performed using Enrichr (98) via the enrichR R package (v.3.0). Heatmaps were generated using the Bioconductor package ComplexHeatmap (v.2.6.2) (99) using log₂-transformed CPM (counts per million) values (values shown are log₂-transformed and row-normalized). Volcano plots were generated using the Bioconductor package EnhancedVolcano (v.1.8.0).

Statistical analysis

Fluorescence values from gated populations in flow cytometry experiments were background corrected by unstained controls and normalized to the values of the cell line harboring negative control sgRNA when appropriate. Normalized data were then grouped by the Cochran method (100), and values for cell lines transduced with individual sgRNAs were compared with those of the negative control by *t* test with Holm-Sidak correction. For direct comparison of flow cytometry populations, the T_{χ} metric was also used (101). For comparison of one-phase decay regression curves in mRNA decay experiments, the extra sum-of-squares *F* test was used. Pairwise testing to controls was performed in all other experiments using Welch's *t* test with Holm-Sidak correction unless otherwise noted. For comparison across more than two groups, one-way analysis of variance (ANOVA) with Tukey's multiple comparisons test or two-way ANOVA with Sidak's multiple comparisons test was used unless otherwise noted. When parametric tests were used, data were tested for normality by the D'Agostino-Pearson or Kolmogorov-Smirnov tests. Adjusted *P* values of <0.05 (two-sided testing) were considered significant. Unless otherwise noted, error bars indicate 95% confidence intervals. In figures, n.s. indicates nonsignificant at *P* > 0.05, **P* < 0.05, ***P* < 0.01, ****P* < 0.001, and *****P* < 0.0001. Statistical analysis was performed using Prism 7 (GraphPad). All experiments were biologically replicated thrice unless otherwise noted.

SUPPLEMENTARY MATERIALS

www.science.org/doi/10.1126/scitranslmed.abbj8670

Materials and Methods

Figs. S1 to S22

Tables S1 to S14

Data file S1

MDAR Reproducibility Checklist

References (102–106)

[View/request a protocol for this paper from Bio-protocol.](#)

REFERENCES AND NOTES

- M. S. Brown, J. L. Goldstein, A receptor-mediated pathway for cholesterol homeostasis. *Science* **232**, 34–47 (1986).
- J. L. Goldstein, M. S. Brown, A century of cholesterol and coronaries: From plaques to genes to statins. *Cell* **161**, 161–172 (2015).
- M. G. Silverman, B. A. Ference, K. Im, S. D. Wiviott, R. P. Giugliano, S. M. Grundy, E. Braunwald, M. S. Sabatine, Association between lowering LDL-C and cardiovascular risk reduction among different therapeutic interventions. *JAMA* **316**, 1289–1297 (2016).
- K. D. Kochanek, J. Xu, E. Arias, Mortality in the United States, 2019. *NCHS Data Brief* **395**, 1–8 (2020).
- M. S. Sabatine, R. P. Giugliano, A. C. Keech, N. Honarpour, S. D. Wiviott, S. A. Murphy, J. F. Kuder, H. Wang, T. Liu, S. M. Wasserman, P. S. Sever, T. R. Pedersen; FOURIER Steering Committee and Investigators, Evolocumab and clinical outcomes in patients with cardiovascular disease. *N. Engl. J. Med.* **376**, 1713–1722 (2017).
- C. Ma, M. E. Gurof, Z. Huang, A. H. Lichtenstein, X. Wang, Y. Wang, S. Neumann, S. Wu, X. Gao, Low-density lipoprotein cholesterol and risk of intracerebral hemorrhage. *Neurology* **93**, e445–e457 (2019).
- M. S. Sabatine, S. D. Wiviott, K. Im, S. A. Murphy, R. P. Giugliano, Efficacy and safety of further lowering of low-density lipoprotein cholesterol in patients starting with very low levels: A meta-analysis. *JAMA Cardiol.* **3**, 823–828 (2018).
- A. Garg, S. Fazio, P. B. Duell, A. Baass, C. Udata, T. Joh, T. Riel, M. Sirota, D. Dettling, H. Liang, P. D. Garzone, B. Gumbiner, H. Wan, Molecular characterization of familial hypercholesterolemia in a North American cohort. *J. Endocr. Soc.* **4**, bvz015 (2019).
- D. Klarin, S. M. Damrauer, K. Cho, Y. V. Sun, T. M. Teslovich, J. Honerlaw, D. R. Gagnon, S. L. DuVall, J. Li, G. M. Peloso, M. Chaffin, A. M. Small, J. Huang, H. Tang, J. A. Lynch, Y.-L. Ho, D. J. Liu, C. A. Emdin, A. H. Li, J. E. Huffman, J. S. Lee, P. Natarajan, R. Chowdhury, D. Saleheen, M. Vujkovic, A. Baras, S. Pyrajan, E. Di Angelantonio, B. M. Neale, A. Naheed, A. V. Khera, J. Danesh, K.-M. Chang, G. Abecasis, C. Willer, F. E. Dewey, D. J. Carey; Global Lipids Genetics Consortium; Myocardial Infarction Genetics (MIGen) Consortium; Geisinger-Regeneron DiscovEHR Collaboration; VA Million Veteran Program, J. Concato, J. M. Gaziano, C. J. O'Donnell, P. S. Tsao, S. Kathiresan, D. J. Rader, P. W. F. Wilson, T. L. Assimes, Genetics of blood lipids among ~300,000 multi-ethnic participants of the Million Veteran Program. *Nat. Genet.* **50**, 1514–1523 (2018).
- P. J. Talmud, S. Shah, R. Whittall, M. Futema, P. Howard, J. A. Cooper, S. C. Harrison, K. Li, F. Drenos, F. Karpe, H. A. W. Neil, O. S. Descamps, C. Langenberg, N. Lench, M. Kivimaki, J. Whittaker, A. D. Hingorani, M. Kumari, S. E. Humphries, Use of low-density lipoprotein cholesterol gene score to distinguish patients with polygenic and monogenic familial hypercholesterolaemia: A case-control study. *Lancet* **381**, 1293–1301 (2013).
- M. T. Oetjens, M. A. Kelly, A. C. Sturm, C. L. Martin, D. H. Ledbetter, Quantifying the polygenic contribution to variable expressivity in eleven rare genetic disorders. *Nat. Commun.* **10**, 4897 (2019).
- L. A. Gilbert, M. A. Horlbeck, B. Adamson, J. E. Villalta, Y. Chen, E. H. Whitehead, C. Guimaraes, B. Panning, H. L. Ploegh, M. C. Bassik, L. S. Qi, M. Kampmann, J. S. Weissman, Genome-scale CRISPR-mediated control of gene repression and activation. *Cell* **159**, 647–661 (2014).
- M. A. Horlbeck, L. A. Gilbert, J. E. Villalta, B. Adamson, R. A. Pak, Y. Chen, A. P. Fields, C. Y. Park, J. E. Corn, M. Kampmann, J. S. Weissman, Compact and highly active next-generation libraries for CRISPR-mediated gene repression and activation. *eLife* **5**, e19760 (2016).
- B. Adamson, T. M. Norman, M. Jost, M. Y. Cho, J. K. Nuñez, Y. Chen, J. E. Villalta, L. A. Gilbert, M. A. Horlbeck, M. Y. Hein, R. A. Pak, A. N. Gray, C. A. Gross, A. Dixit, O. Parnas, A. Regev, J. S. Weissman, A multiplexed single-cell CRISPR screening platform enables systematic dissection of the unfolded protein response. *Cell* **167**, 1867–1882.e21 (2016).
- K. K. Ray, R. S. Wright, D. Kallend, W. Koenig, L. A. Leiter, F. J. Raal, J. A. Bisch, T. Richardson, M. Jaros, P. L. J. Wijngaard, J. J. P. Kastelein; ORION-10 and ORION-11 Investigators, Two phase 3 trials of inclisiran in patients with elevated LDL cholesterol. *N. Engl. J. Med.* **382**, 1507–1519 (2020).
- B. B. Knowles, C. C. Howe, D. P. Aden, Human hepatocellular carcinoma cell lines secrete the major plasma proteins and hepatitis B surface antigen. *Science* **209**, 497–499 (1980).
- H. Schrnagl, R. Schinker, H. Gierens, M. Nauck, H. Wieland, W. März, Effect of atorvastatin, simvastatin, and lovastatin on the metabolism of cholesterol and triacylglycerides in HepG2 cells. *Biochem. Pharmacol.* **62**, 1545–1555 (2001).
- J. Liu, F. Zhang, C. Li, M. Lin, M. R. Briggs, Synergistic activation of human LDL receptor expression by SCAP ligand and cytokine oncostatin M. *Arterioscler. Thromb. Vasc. Biol.* **23**, 90–96 (2003).
- G. Dubuc, A. Chamberland, H. Wassef, J. Davignon, N. G. Seidah, L. Bernier, A. Prat, Statins upregulate PCSK9, the gene encoding the proprotein convertase neural apoptosis-regulated convertase-1 implicated in familial hypercholesterolemia. *Arterioscler. Thromb. Vasc. Biol.* **24**, 1454–1459 (2004).
- T. A. Lagace, D. E. Curtis, R. Garuti, M. C. McNutt, S. W. Park, H. B. Prather, N. N. Anderson, Y. K. Ho, R. E. Hammer, J. D. Horton, Secreted PCSK9 decreases the number of LDL receptors in hepatocytes and in livers of parabiotic mice. *J. Clin. Invest.* **116**, 2995–3005 (2006).
- M. S. Brown, J. R. Faust, J. L. Goldstein, I. Kaneko, A. Endo, Induction of 3-hydroxy-3-methylglutaryl coenzyme A reductase activity in human fibroblasts incubated with compactin (ML-236B), a competitive inhibitor of the reductase. *J. Biol. Chem.* **253**, 1121–1128 (1978).
- S. Benjannet, D. Rhainds, R. Essalmani, J. Mayne, L. Wickham, W. Jin, M.-C. Asselin, J. Hamelin, M. Varret, D. Allard, M. Trillard, M. Abifadel, A. Tebon, A. D. Attie, D. J. Rader, C. Boileau, L. Brissette, M. Chrétiens, A. Prat, N. G. Seidah, NARC-1/PCSK9 and its natural mutants: Zymogen cleavage and effects on the low density lipoprotein (LDL) receptor and LDL cholesterol. *J. Biol. Chem.* **279**, 48865–48875 (2004).
- S. Rashid, D. E. Curtis, R. Garuti, N. N. Anderson, Y. Bashmakov, Y. K. Ho, R. E. Hammer, Y. A. Moon, J. D. Horton, Decreased plasma cholesterol and hypersensitivity to statins in mice lacking Pcsk9. *Proc. Natl. Acad. Sci. U.S.A.* **102**, 5374–5379 (2005).

47. S. F. Parsons, G. Mallinson, C. H. Holmes, J. M. Houlihan, K. L. Simpson, W. J. Mawby, N. K. Spurr, D. Warne, A. N. Barclay, D. J. Anstee, The Lutheran blood group glycoprotein, another member of the immunoglobulin superfamily, is widely expressed in human tissues and is developmentally regulated in human liver. *Proc. Natl. Acad. Sci. U.S.A.* **92**, 5496–5500 (1995).
48. S. K. Mishra, P. A. Keyel, M. A. Edeling, A. L. Dupin, D. J. Owen, L. M. Traub, Functional dissection of an AP-2 β 2 appendage-binding sequence within the autosomal recessive hypercholesterolemia protein. *J. Biol. Chem.* **280**, 19270–19280 (2005).
49. Scandinavian Simvastatin Survival Study Group, Randomised trial of cholesterol lowering in 4444 patients with coronary heart disease: The Scandinavian Simvastatin Survival Study (4S). *Lancet* **344**, 1383–1389 (1994).
50. N. G. Lintner, K. F. McClure, D. Petersen, A. T. Londregan, D. W. Piotrowski, L. Wei, J. Xiao, M. Bolt, P. M. Loria, B. Maguire, K. F. Geoghegan, A. Huang, T. Rolph, S. Liras, J. A. Doudna, R. G. Dullea, J. H. D. Cate, Selective stalling of human translation through small-molecule engagement of the ribosome nascent chain. *PLoS Biol.* **15**, e2001882 (2017).
51. H. E. Careskey, R. A. Davis, W. E. Alborn, J. S. Troutt, G. Cao, R. J. Konrad, Atorvastatin increases human serum levels of proprotein convertase subtilisin/kexin type 9. *J. Lipid Res.* **49**, 394–398 (2008).
52. T. Suzuki, M. Terasaki, C. Takemoto-Hori, T. Hanada, T. Ueda, A. Wada, K. Watanabe, Structural compensation for the deficit of rRNA with proteins in the mammalian mitochondrial ribosome. Systematic analysis of protein components of the large ribosomal subunit from mammalian mitochondria. *J. Biol. Chem.* **276**, 21724–21736 (2001).
53. P. J. Thul, L. Akesson, M. Wiking, D. Mahdessian, A. Geladaki, H. A. Blal, T. Alm, A. Asplund, L. Björk, L. M. Breckels, A. Bäckström, F. Danielsson, L. Fagerberg, J. Fall, L. Gatto, C. Gnann, S. Hober, M. Hjelmare, F. Johansson, S. Lee, C. Lindskog, J. Mulder, C. M. Mulvey, P. Nilsson, P. Oksvold, J. Rockberg, R. Schütten, J. M. Schwenk, A. Sivertsson, E. Sjöstedt, M. Skogs, C. Stadler, D. P. Sullivan, H. Tegel, C. Winsnes, C. Zhang, M. Zwaan, A. Mardinoglu, F. Pontén, K. Von Feilitzen, K. S. Lilley, M. Uhlen, E. Lundberg, A subcellular map of the human proteome. *Science* **356**, eaal3321 (2017).
54. H. Li, B. Dong, S. W. Park, H.-S. Lee, W. Chen, J. Liu, Hepatocyte nuclear factor 1 α plays a critical role in PCSK9 gene transcription and regulation by the natural hypocholesterolemic compound berberine. *J. Biol. Chem.* **284**, 28885–28895 (2009).
55. A.-X. Guo, J.-J. Cui, L.-Y. Wang, J.-Y. Yin, The role of CSDE1 in translational reprogramming and human diseases. *Cell Commun. Signal* **18**, 14 (2020).
56. M. Dinur, R. Kilav, A. Sela-Brown, H. Jacquemin-Sablon, T. Naveh-Many, In vitro evidence that upstream of N-ras participates in the regulation of parathyroid hormone messenger ribonucleic acid stability. *Mol. Endocrinol.* **20**, 1652–1660 (2006).
57. K. S. Moore, N. Yagci, F. Van Alphen, N. A. Paolini, R. Horos, N. M. Held, R. H. Houtkooper, E. Van Den Akker, A. B. Meijer, P. A. C. T'Hoën, M. Von Lindern, Csde1 binds transcripts involved in protein homeostasis and controls their expression in an erythroid cell line. *Sci. Rep.* **8**, 2628 (2018).
58. T. C. Chang, A. Yamashita, C. Y. A. Chen, Y. Yamashita, W. Zhu, S. Durdan, A. Kahvejian, N. Sonenberg, A. Bin Shyu, UNR, a new partner of poly(A)-binding protein, plays a key role in translationally coupled mRNA turnover mediated by the c-fos major coding-region determinant. *Genes Dev.* **18**, 2010–2023 (2004).
59. G. M. Wilson, M. Z. Vasa, R. G. Deeley, Stabilization and cytoskeletal-association of LDL receptor mRNA are mediated by distinct domains in its 3' untranslated region. *J. Lipid Res.* **39**, 1025–1032 (1998).
60. M. A. Horlbeck, A. Xu, M. Wang, N. K. Bennett, C. Y. Park, D. Bogdanoff, B. Adamson, E. D. Chow, M. Kampmann, T. R. Peterson, K. Nakamura, M. A. Fischbach, J. S. Weissman, L. A. Gilbert, Mapping the genetic landscape of human cells. *Cell* **174**, 953–967.e22 (2018).
61. H. Li, W. Chen, Y. Zhou, P. Abidi, O. Sharpe, W. H. Robinson, F. B. Kraemer, J. Liu, Identification of mRNA binding proteins that regulate the stability of LDL receptor mRNA through AU-rich elements. *J. Lipid Res.* **50**, 820–831 (2009).
62. K. Bjune, L. Wierød, S. Naderi, Triciribine increases LDLR expression and LDL uptake through stabilization of LDLR mRNA. *Sci. Rep.* **8**, 16174 (2018).
63. T. Bakheet, M. Frevel, B. R. G. Williams, W. Greer, K. S. A. Khabar, ARED: Human AU-rich element-containing mRNA database reveals an unexpectedly diverse functional repertoire of encoded proteins. *Nucleic Acids Res.* **29**, 246–254 (2001).
64. C. Liu, Y. S. Kim, J. Kim, J. Pattison, A. Kamaid, Y. I. Miller, Modeling hypercholesterolemia and vascular lipid accumulation in LDL receptor mutant zebrafish. *J. Lipid Res.* **59**, 391–399 (2018).
65. R. S. Wu, I. I. Lam, H. Clay, D. N. Duong, R. C. Deo, S. R. Coughlin, A rapid method for directed gene knockout for screening in G0 zebrafish. *Dev. Cell* **46**, 112–125.e4 (2018).
66. A. B. Singh, H. Li, C. F. K. Kan, B. Dong, M. R. Nicolis, J. Liu, The critical role of mRNA destabilizing protein heterogeneous nuclear ribonucleoprotein D in 3' untranslated region-mediated decay of low-density lipoprotein receptor mRNA in liver tissue. *Arterioscler. Thromb. Vasc. Biol.* **34**, 8–16 (2014).
67. B. Paigen, A. Morrow, C. Brandon, D. Mitchell, P. Holmes, Variation in susceptibility to atherosclerosis among inbred strains of mice. *Atherosclerosis* **57**, 65–73 (1985).
68. A. H. Lichtman, S. K. Clinton, K. Iiyama, P. W. Connelly, P. Libby, M. I. Cybulsky, Hyperlipidemia and atherosclerotic lesion development in LDL receptor-deficient mice fed defined semipurified diets with and without cholate. *Arterioscler. Thromb. Vasc. Biol.* **19**, 1938–1944 (1999).
69. G. S. Getz, C. A. Reardon, Diet and murine atherosclerosis. *Arterioscler. Thromb. Vasc. Biol.* **26**, 242–249 (2006).
70. M. von Scheidt, Y. Zhao, Z. Kurt, C. Pan, L. Zeng, X. Yang, H. Schunkert, A. J. Lusis, Applications and limitations of mouse models for understanding human atherosclerosis. *Cell Metab.* **25**, 248–261 (2017).
71. M. M. Björklund, A. K. Hollensen, M. K. Hagensen, F. Dagnæs-Hansen, C. Christoffersen, J. G. Mikkelsen, J. F. Bentzon, Induction of atherosclerosis in mice and hamsters without germline genetic engineering. *Circ. Res.* **114**, 1684–1689 (2014).
72. R. P. Giugliano, T. R. Pedersen, J.-G. Park, G. M. De Ferrari, Z. A. Gaciong, R. Ceska, K. Toth, I. Gouni-Berthold, J. Lopez-Miranda, F. Schiele, F. Mach, B. R. Ott, E. Kanevsky, A. L. Pineda, R. Somaratne, S. M. Wasserman, A. C. Keech, P. S. Sever, M. S. Sabatine; FOURIER Investigators, Clinical efficacy and safety of achieving very low LDL-cholesterol concentrations with the PCSK9 inhibitor evolocumab: A prespecified secondary analysis of the FOURIER trial. *Lancet* **390**, 1962–1971 (2017).
73. B. T. Emmer, E. J. Sherman, P. J. Lascuna, S. E. Graham, C. J. Willer, D. Ginsburg, Genome-scale CRISPR screening for modifiers of cellular LDL uptake. *PLOS Genet.* **17**, e1009285 (2021).
74. M. N. Trinh, M. S. Brown, J. L. Goldstein, J. Han, G. Vale, J. G. McDonald, J. Seemann, J. T. Mendell, F. Lu, Last step in the path of LDL cholesterol from lysosome to plasma membrane to ER is governed by phosphatidyserine. *Proc. Natl. Acad. Sci. U.S.A.* **117**, 18521–18529 (2020).
75. C. Knouff, S. Malloy, J. Wilder, M. K. Altenburg, N. Maeda, Doubling expression of the low density lipoprotein receptor by truncation of the 3'-untranslated region sequence ameliorates type III hyperlipoproteinemia in mice expressing the human ApoE2 isoform. *J. Biol. Chem.* **276**, 3856–3862 (2001).
76. E. Björnsson, K. Gunnarsdóttir, G. H. Halldorsson, A. Sigurdsson, G. A. Arnadóttir, H. Jonsson, E. F. Olafsdóttir, S. Niehus, B. Kehr, G. Sveinbjörnsson, S. Gudmundsdóttir, A. Helgadóttir, K. Andersen, G. Thorleifsson, G. I. Eyjólfsson, I. Olafsson, O. Sigurdardóttir, J. Saemundsdóttir, I. Jonsdóttir, O. T. Magnusson, G. Masson, H. Stefansson, D. F. Gudbjartsson, G. Thorgerirsson, H. Holm, B. V. Halldorsson, P. Melsted, G. L. Norddahl, P. Sulem, U. Thorsteinsdóttir, K. Stefansson, Lifelong reduction in LDL (low-density lipoprotein) cholesterol due to a gain-of-function mutation in LDLR. *Circ. Genomic Precis. Med.* **14**, e003029 (2021).
77. W. Kong, J. Wei, P. Abidi, M. Lin, S. Inaba, C. Li, Y. Wang, Z. Wang, S. Si, H. Pan, S. Wang, J. Wu, Y. Wang, Z. Li, J. Liu, J. D. Jiang, Berberine is a novel cholesterol-lowering drug working through a unique mechanism distinct from statins. *Nat. Med.* **10**, 1344–1351 (2004).
78. M. Dandan, J. Han, S. Mann, R. Kim, H. Mohammed, E. Nyangau, M. Hellerstein, Turnover rates of the low-density lipoprotein receptor and PCSK9: Added dimension to the cholesterol homeostasis model. *Arterioscler. Thromb. Vasc. Biol.* **41**, 2866–2876 (2021).
79. A. B. Singh, C. F. K. Kan, V. Shende, B. Dong, J. Liu, A novel posttranscriptional mechanism for dietary cholesterol-mediated suppression of liver LDL receptor expression. *J. Lipid Res.* **55**, 1397–1407 (2014).
80. H. J. Lee, D. Bartsch, C. Xiao, S. Guerrero, G. Ahuja, C. Schindler, J. J. Moresco, J. R. Yates III, F. Gebauer, H. Bazzi, C. Dieterich, L. Kurian, D. Vilchez, A post-transcriptional program coordinated by CSDE1 prevents intrinsic neural differentiation of human embryonic stem cells. *Nat. Commun.* **8**, 1456 (2017).
81. O. Boussadia, M. Niepmann, L. Créancier, A.-C. Prats, F. Dautry, H. Jacquemin-Sablon, Unr is required in vivo for efficient initiation of translation from the internal ribosome entry sites of both rhinovirus and poliovirus. *J. Virol.* **77**, 3353–3359 (2003).
82. V. Dormoy-Raclet, J. Markovits, A. Jacquemin-Sablon, H. Jacquemin-Sablon, Regulation of Unr expression by 5' and 3'-untranslated regions of its mRNA through modulation of stability and IRES mediated translation. *RNA Biol.* **2**, e27–e35 (2005).
83. K. E. Duncan, C. Strein, M. W. Hentze, The SXL-UNR corepressor complex uses a PABP-mediated mechanism to inhibit ribosome recruitment to msl-2 mRNA. *Mol. Cell* **36**, 571–582 (2009).
84. H. Guo, Y. Li, L. Shen, T. Wang, X. Jia, L. Liu, T. Xu, M. Ou, K. Hoekzema, H. Wu, M. A. Gillentine, C. Liu, H. Ni, P. Peng, R. Zhao, Y. Zhang, C. Phornphutkul, A. P. A. Stegmann, C. E. Prada, R. J. Hopkin, J. T. Shieh, K. McWalter, K. G. Monaghan, P. M. van Hasselt, K. van Gassen, T. Bai, M. Long, L. Han, Y. Quan, M. Chen, Y. Zhang, K. Li, Q. Zhang, J. Tan, T. Zhu, Y. Liu, N. Pang, J. Peng, D. A. Scott, S. R. Lalani, M. Azamian, G. M. S. Mancini, D. J. Adams, M. Kvarnung, A. Lindstrand, A. Nordgren, J. Pevsner, I. A. Osei-Owusu, C. Romano, G. Calabrese, O. Galesi, J. Gecz, E. Haan, J. Ranells, M. Racobaldo, M. Nordenskjöld, S. Madan-Khetarpal, J. Sebastian, S. Ball, X. Zou, J. Zhao, Z. Hu, F. Xia, P. Liu, J. A. Rosenfeld, B. B. A. de Vries, R. A. Bernier, Z. Q. D. Xu, H. Li, W. Xie, R. B. Hufnagel, E. E. Eichler, K. Xia, Disruptive variants of CSDE1 associate with autism

- and interfere with neuronal development and synaptic transmission. *Sci. Adv.* **5**, eaax2166 (2019).
85. L. Wurth, P. Papasaiikas, D. Olmeda, N. Bley, G. T. Calvo, S. Guerrero, D. Cerezo-Wallis, J. Martinez-Useros, M. García-Fernández, S. Hüttelmaier, M. S. Soengas, F. Gebauer, UNR/CSDE1 drives a post-transcriptional program to promote melanoma invasion and metastasis. *Cancer Cell* **30**, 694–707 (2016).
 86. P. Genenemark, K. Walter, N. Clemmensen, D. Rekić, C. A. M. Nilsson, J. Knöchel, M. Hölttä, L. Wernevik, B. Rosengren, D. Kakol-Palm, Y. Wang, R. Z. Yu, R. S. Geary, S. J. Riney, B. P. Monia, R. Isaksson, R. Jansson-Löfmark, C. S. J. Rocha, D. Lindén, E. Hurt-Camejo, R. Crooke, L. Tillman, T. Rydén-Bergsten, B. Carlsson, U. Andersson, M. Elebring, A. Tivesten, N. Davies, An oral antisense oligonucleotide for PCSK9 inhibition. *Sci. Transl. Med.* **13**, eabe9117 (2021).
 87. K. Musunuru, A. C. Chadwick, T. Mizoguchi, S. P. Garcia, J. E. DeNizio, C. W. Reiss, K. Wang, S. Iyer, C. Dutta, V. Clendaniel, M. Amaonye, A. Beach, K. Berth, S. Biswas, M. C. Braun, H.-M. Chen, T. V. Colace, J. D. Ganey, S. A. Gangopadhyay, R. Garrity, L. N. Kasiewicz, J. Lavoie, J. A. Madsen, Y. Matsumoto, A. M. Mazzola, Y. S. Nasrullah, J. Nneji, H. Ren, A. Sanjeev, M. Shay, M. R. Stahley, S. H. Y. Fan, Y. K. Tam, N. M. Gaudelli, G. Ciaramella, L. E. Stolz, P. Malyala, C. J. Cheng, K. G. Rajeev, E. Rohde, A. M. Bellinger, S. Kathiresan, In vivo CRISPR base editing of PCSK9 durably lowers cholesterol in primates. *Nature* **593**, 429–434 (2021).
 88. K. F. McClure, D. W. Piotrowski, D. Petersen, L. Wei, J. Xiao, A. T. Londregan, A. S. Kamlet, A.-M. Dechert-Schmitt, B. Raymer, R. B. Ruggeri, D. Canterbury, C. Limberakis, S. Liras, P. DaSilva-Jardine, R. G. Dullea, P. M. Loria, B. Reidich, C. T. Salatto, H. Eng, E. Kimoto, K. Atkinson, A. King-Ahmad, D. Scott, K. Beaumont, J. R. Chabot, M. W. Bolt, K. Maresca, K. Dahl, R. Arakawa, A. Takano, C. Halldin, Liver-targeted small-molecule inhibitors of proprotein convertase subtilisin/kexin type 9 synthesis. *Angew. Chemie Int. Ed.* **56**, 16218–16222 (2017).
 89. J. J. V. McMurray, M. Packer, A. S. Desai, J. Gong, M. P. Lefkowitz, A. R. Rizkala, J. L. Rouleau, V. C. Shi, S. D. Solomon, K. Swedberg, M. R. Zile; PARADIGM-HF Investigators and Committees, Angiotensin–neprilysin inhibition versus enalapril in heart failure. *N. Engl. J. Med.* **371**, 993–1004 (2014).
 90. C. Sudlow, J. Gallacher, N. Allen, V. Beral, P. Burton, J. Danesh, P. Downey, P. Elliott, J. Green, M. Landray, B. Liu, P. Matthews, G. Ong, J. Pell, A. Silman, A. Young, T. Sprosen, T. Peakman, R. Collins, UK Biobank: An open access resource for identifying the causes of a wide range of complex diseases of middle and old age. *PLoS Med.* **12**, e1001779 (2015).
 91. P. R. Loh, G. Tucker, B. K. Bulik-Sullivan, B. J. Vilhjálmsson, H. K. Finucane, R. M. Salem, D. I. Chasman, P. M. Ridker, B. M. Neale, B. Berger, N. Patterson, A. L. Price, Efficient Bayesian mixed-model analysis increases association power in large cohorts. *Nat. Genet.* **47**, 284–290 (2015).
 92. J. M. Baker, F. M. Boyce, High-throughput functional screening using a homemade dual-glow luciferase assay. *J. Vis. Exp.* **88**, e50282 (2014).
 93. J. S. Chorbha, A. M. Galvan, K. M. Shokat, Stepwise processing analyses of the single-turnover PCSK9 protease reveal its substrate sequence specificity and link clinical genotype to lipid phenotype. *J. Biol. Chem.* **293**, 1875–1886 (2018).
 94. J. S. Chorbha, A. M. Galvan, K. M. Shokat, A high-throughput luciferase assay to evaluate proteolysis of the single-turnover protease PCSK9. *J. Vis. Exp.* **138**, e58265 (2018).
 95. M. I. Love, W. Huber, S. Anders, Moderated estimation of fold change and dispersion for RNA-seq data with DESeq2. *Genome Biol.* **15**, 550 (2014).
 96. M. D. Robinson, D. J. McCarthy, G. K. Smyth, edgeR: A Bioconductor package for differential expression analysis of digital gene expression data. *Bioinformatics* **26**, 139–140 (2010).
 97. A. T. L. Lun, Y. Chen, G. K. Smyth, It's DE-licious: A recipe for differential expression analyses of RNA-seq experiments using quasi-likelihood methods in edgeR. *Methods Mol. Biol.* **1418**, 391–416 (2016).
 98. M. V. Kuleshov, M. R. Jones, A. D. Rouillard, N. F. Fernandez, Q. Duan, Z. Wang, S. Koplev, S. L. Jenkins, K. M. Jagodnik, A. Lachmann, M. G. McDermott, C. D. Monteiro, G. W. Gunderen, A. Ma'ayan, Enrichr: A comprehensive gene set enrichment analysis web server 2016 update. *Nucleic Acids Res.* **44**, W90–W97 (2016).
 99. Z. Gu, R. Eils, M. Schlesner, Complex heatmaps reveal patterns and correlations in multidimensional genomic data. *Bioinformatics* **32**, 2847–2849 (2016).
 100. J. P. T. Higgins, S. Green, *Cochrane Handbook for Systematic Reviews of Interventions version 5.1.0* (The Cochrane Collaboration, 2011).
 101. M. Roederer, W. Moore, A. Treister, R. R. Hardy, L. A. Herzenberg, Probability binning comparison: A metric for quantitating multivariate distribution differences. *Cytometry* **45**, 47–55 (2001).
 102. D. G. Gibson, L. Young, R.-Y. Chuang, J. C. Venter, C. A. Hutchison III, H. O. Smith, Enzymatic assembly of DNA molecules up to several hundred kilobases. *Nat. Methods* **6**, 343–345 (2009).
 103. J. H. Kim, S.-R. Lee, L.-H. Li, H.-J. Park, J.-H. Park, K. Y. Lee, M.-K. Kim, B. A. Shin, S.-Y. Choi, High cleavage efficiency of a 2A peptide derived from porcine teschovirus-1 in human cell lines, zebrafish and mice. *PLoS ONE* **6**, e18556 (2011).
 104. D. G. Gibson, H. O. Smith, C. A. Hutchison III, J. C. Venter, C. Merryman, Chemical synthesis of the mouse mitochondrial genome. *Nat. Methods* **7**, 901–903 (2010).
 105. UniProt Consortium, UniProt: A worldwide hub of protein knowledge. *Nucleic Acids Res.* **47**, D506–D515 (2019).
 106. A. Padmanabhan, M. Alexanian, R. Linares-Saldana, B. González-Terán, G. Andreoletti, Y. Huang, A. J. Connolly, W. Kim, A. Hsu, Q. Duan, S. A. B. Winchester, F. Felix, J. A. Perez-Bermejo, Q. Wang, L. Li, P. P. Shah, S. M. Haldar, R. Jain, D. Srivastava, BRD4 (bromodomain-containing protein 4) interacts with GATA4 (GATA binding protein 4) to govern mitochondrial homeostasis in adult cardiomyocytes. *Circulation* **142**, 2338–2355 (2020).

Acknowledgments: We thank M. Horlbeck for guidance with the CRISPRi system, J. D. Brown for helpful discussion on in vivo experimental designs, R. Yang for assistance with histologic imaging, and P. Cheng and R. Baylis for helpful discussion on histologic insights and in vivo experimental planning. Plasmids for the CRISPRi system were a gift from L. Gilbert and J. Weissman. We thank the Gladstone Institutes Flow Cytometry core facility for assistance with flow cytometry experiments. UK Biobank analyses were conducted using the UK Biobank resource under application 7089. **Funding:** This work was supported by grants from the Tobacco-Related Disease Research Program (578649 to A. Padmanabhan), the A.P. Giannini Foundation (P0527061 to A. Padmanabhan), the Michael Antonov Charitable Foundation Inc. to A. Padmanabhan, the Sarnoff Cardiovascular Research Foundation to A. Padmanabhan, the Japan Society for the Promotion of Science Overseas Research Fellowship to T.N., the Burroughs Wellcome Foundation to R.J., a Hassenfeld Scholar Award from the Massachusetts General Hospital to P.N., the Fondation Leducq (TNE-18CVD04 to P.N.), the Roddenberry Foundation to D.S., the L.K. Whittier Foundation to D.S., the Younger Family Fund to D.S., the Howard Hughes Medical Institute to K.M.S., a Pfizer ASPIRE Cardiovascular Award to J.S.C., the Harris Fund and Research Evaluation and Allocation Committee of the UCSF School of Medicine to J.S.C., the NIH/NCRR (C06 RR018928 to the Gladstone Institute and D.S.), and the NIH/NHLBI (K08 HL157700 to A. Padmanabhan, R01 HL139783 to R.J., R01 HL127564 to P.N., R01 HL142711 to P.N., R01 HL148565 to P.N., R01 HL148050 to P.N., R01 DK119621 to B.L.B., P01 HL146366 to B.L.B. and D.S., P01 HL098707 to D.S., R01 HL057181 to D.S., R01 HL127240 to D.S., K08 HL124068 to J.S.C., R03 HL145259 to J.S.C., R01 HL146404 to J.S.C., and R01 HL159457 to J.S.C.). **Author contributions:** Overall study design: J.S.C. Execution of in vitro screen and data processing: G.A.S. Genomic analyses: A. Pampana and P.N. In vitro validation and synergy experiments and analysis of mouse blood samples: J.S.C. Execution of zebrafish gene knockdowns: B.H.L. and R.S.W. Oversight of zebrafish husbandry: R.S.W. and B.L.B. Planning and execution of in vivo mouse experiments: A. Padmanabhan. Mouse handling and blood and tissue collection and analysis: A. Padmanabhan, C.Y.L., T.N., N.S., and V.Q.X. Processing of RNA-seq data: A. Padmanabhan and A. Pelonero. Histologic analysis of mouse samples: L.L. and R.J. Critical data review and analysis: B.L.B., D.S., and K.M.S. Preparation of the manuscript: J.S.C. Critical review and revision of the manuscript: All authors. **Competing interests:** P.N. reports investigator-initiated grant support from Amgen, Apple, AstraZeneca, Boston Scientific, and Novartis; personal fees from Apple, AstraZeneca, Blackstone Life Sciences, Foresite Labs, Novartis, and Roche/Genentech; is a cofounder of TenSixteen Bio; is a shareholder of geneXwell and TenSixteen Bio; and spousal employment at Vertex, all unrelated to the present work. R.S.W. is an employee of Amgen Inc. D.S. is the scientific cofounder, shareholder, and director of Tenaya Therapeutics, unrelated to the present work. K.M.S. has consulting agreements for the following companies involving cash and/or stock compensation: Black Diamond Therapeutics, BridGene Biosciences, Denali Therapeutics, Dice Molecules, eFFECTOR Therapeutics, Erasca, Genentech/Roche, Janssen Pharmaceuticals, Kumquat Biosciences, Kura Oncology, Merck, Mitokinin, Petra Pharma, Revolution Medicines, Type6 Therapeutics, Venthera, and Wellspring Biosciences (Araxes Pharma). J.S.C. has received consulting fees from Gilde Healthcare and is an uncompensated scientific advisor to Eko, both unrelated to this work. **Data and materials availability:** All data associated with this study are present in the paper or the Supplementary Materials. All requests for materials, including plasmids or cell lines, generated in this study are available from the corresponding author via material transfer agreement. UK Biobank data are available by application to the UK Biobank. The raw and processed sequencing data from the RNA-seq experiments have been deposited in the Gene Expression Omnibus (GEO) database under the accession number GSE206846.

Submitted 7 June 2021
Resubmitted 13 May 2022
Accepted 25 August 2022
Published 14 September 2022
10.1126/scitranslmed.abj8670

Cold shock domain–containing protein E1 is a posttranscriptional regulator of the LDL receptor

Geoffrey A. SmithArun PadmanabhanBryan H. LauAkhil PampanaLi LiClara Y. LeeAngelo PeloneroTomohiro NishinoNandhini SadagopanVivian Q. XiaRajan JainPradeep NatarajanRoland S. WuBrian L. BlackDeepak SrivastavaKevan M. ShokatJohn S. Chorba

Sci. Transl. Med., 14 (662), eabj8670. • DOI: 10.1126/scitranslmed.abj8670

Controlling CSDE1 to contain cholesterol levels

Therapies that up-regulate the hepatic low-density lipoprotein receptor (LDLR) have been shown to reduce cholesterol concentrations and lower the risk of heart attacks. However, further lowering of cholesterol concentrations beyond what statins can achieve may potentially further reduce heart attack risk. Here, Smith and colleagues conducted a genome-wide CRISPR interference screen to identify further factors involved in hepatic LDLR regulation, identifying cold shock domain–containing protein E1 (CSDE1) as a posttranslational regulator of the stability of *LDLR* mRNA. Knockdown of *Csde1* in mice protected the animals from cholesterol accumulation, even on a cholate-rich diet. These findings suggest that CSDE1 may be a therapeutic target to further lower cholesterol in humans.

View the article online

<https://www.science.org/doi/10.1126/scitranslmed.abj8670>

Permissions

<https://www.science.org/help/reprints-and-permissions>

Use of this article is subject to the [Terms of service](#)